Diluted quantum antiferromagnets: Spin excitations and long-range order

A. L. Chernyshev,[1,*] Y. C. Chen,[2] and A. H. Castro Neto[3,†]
[1]*Solid State Division, Oak Ridge National Laboratory, Oak Ridge, Tennessee 37831*
[2]*Department of Physics, University of California, Riverside, California 92521*
[3]*Department of Physics, Boston University, Boston, Massachusetts 02215*
(Received 24 July 2001; published 11 February 2002)

We have studied the static and dynamic magnetic properties of two-dimensional (2D) and quasi-two-dimensional, spin-S, quantum Heisenberg antiferromagnets diluted with spinless vacancies. Using spin-wave theory and the T-matrix approximation we have calculated the staggered magnetization $M(x,T)$, the neutron scattering dynamical structure factor $\mathcal{S}(\mathbf{k},\omega)$, the 2D magnetic correlation length $\xi(x,T)$ and, for the quasi-(2D) case, the Néel temperature $T_N(x)$. We find that in two dimensions a hydrodynamic description of excitations in terms of spin waves breaks down at wavelengths *larger* than $l/a \sim e^{\pi/4x}$, x being the impurity concentration and a the lattice spacing. We find signatures of localization associated with the scale l, and interpret this scale as the localization length of magnons. The spectral function for momenta $a^{-1} \gg k \gg l^{-1}$ consists of two distinct parts: (i) a damped quasiparticle peak at an energy $c_0 k \gtrsim \omega \gg \omega_0$, with abnormal damping $\Gamma_k \sim x\, c_0 k$, where $\omega_0 \sim c_0 l^{-1}$, c_0 is the bare spin-wave velocity; and (ii) a non-Lorentian localization peak at $\omega \sim \omega_0$. For $k \lesssim l^{-1}$ these two structures merge, and the spectrum becomes incoherent. The density of states acquires a constant term, and exhibits an anomalous peak at $\omega \sim \omega_0$ associated with low-energy localized excitations. These anomalies lead to a substantial enhancement of the magnetic specific heat C_M at low temperatures. Although the dynamical properties are significantly modified, we show that $D=2$ is not the lower critical dimension for this problem. We find that at small x the average staggered magnetization at the magnetic site is $M(x,0) \simeq S - \Delta - Bx$, where Δ is the zero-point spin deviation and $B \simeq 0.21$ is independent of the value of S; the Néel temperature $T_N(x) \simeq (1 - A_s\, x)\ \ T_N(0)$, where $A_s = \pi - 2/\pi + B/(S-\Delta)$ is weakly S dependent. Our results are in quantitative agreement with recent Monte Carlo simulations and experimental data for $S=1/2$, 1, and 5/2. In our approach long-range order persists up to a high concentration of impurities x_c which is above the classical percolation threshold $x_p \approx 0.41$. This result suggests that long-range order is stable at small x, and can be lost only around $x \simeq x_p$ where approximations of our approach become invalid.

DOI: 10.1103/PhysRevB.65.104407 PACS number(s): 75.10.Jm, 75.10.Nr, 75.40.Gb

I. INTRODUCTION

The discovery of superconducting cuprates (HTC) has motivated an enormous amount of studies in low-dimensional magnetic systems during the last 15 years.[1–3] However superconducting materials now form only a subfield in the activity of low-D quantum magnetism (see Ref. 4). The hope for an insight into the physics of HTC from a study of magnetically related system has attracted much attention to the properties of diluted two-dimensional, quantum Hersenberg antiferromagnets (QHAF's).[5–27] One such system, $La_2Cu_{1-x}Zn(Mg)_xO_4$ (LCO), a quasi-2D, $S=1/2$, QHAF diluted with spinless vacancies, has been a subject of great interest because of the possibility of quantum critical points (QCP's) in its phase diagram. Earlier experimental data,[17] while demonstrating that LCO shows a much stronger stability against doping in comparison with the mobile-hole-doped compound $La_{2-x}Sr_xCuO_4$, indicated the existence of a QCP at $x=x_c \approx 0.2$, well below the classical percolation threshold. This finding was in sharp contrast with classical magnetic systems where dilution leads to a breaking of the magnetic bonds, and long-range order (LRO) is lost only at the percolation threshold x_p, a characteristic value of the dilution fraction x at which the last infinite cluster of connected spins disappears. For a 2D square lattice, $x_p \approx 0.41$.[28] The existence of such a QCP below the percolation threshold was thought to be possible, given the large amount of quantum fluctuations in the ground state of $S=1/2$ system. However, only recently were a systematic experimental analysis of the diluted 2D AF performed in a wide range of doping.[18–20] Although there were several other experimental realizations of a 2D QHAF on a square lattice with $S=1/2$ (Refs. 21–23) and $S=5/2$,[24,29] the CuO-based compounds are among the few which allow a direct probe via elastic and inelastic neutron scattering. At the same time, quantum Monte Carlo (MC) studies provided highly reliable simulations of large lattices at low temperatures.[25,26] These works indicated that, in fact, no QCP point exists below x_p, and that at percolation threshold the phase transition is characterized by classical exponents.[26,27]

Note that theoretical studies of diluted spin systems attracted much attention some 30 years ago in the context of magnetism in diluted magnetic alloys.[30–33] Most of these studies focused on large-S (classical) Heisenberg or Ising systems. The traditional view of the effect of local disorder on the spectrum of an ordered 3D antiferromagnet is that at long wavelengths the *form* of the spectrum is not modified. The only effects are the reduction of hydrodynamic parameters (spin stiffness, spin-wave velocity, etc.[34]) and a weak damping. Conventional arguments for this ability of the long-wavelength spectrum to withstand perturbations on a local scale often appeal to the Goldstone theorem,[35] although

 ©2002 The American Physical Society

its applicability to systems without translational invariance requires the additional assumption that the microscopic details are virtually averaged on short distances. As a result the low-energy excitations are weakly damped spin waves which belong to a so-called ''infinite cluster,'' and they are well defined up to the percolation threshold.[35] This effective restoration of the translational invariance involves spin-wave propagation on randomly directed paths with some Euclidean distance L' which can be converted to a ''true'' distance L. Thus the wave vector preserves its meaning at long wavelengths.[36] In three dimensions these arguments work very well, and are assumed to demonstrate a ''general principle.''

There is growing evidence that, in two dimensions, such logic is not always valid. In the 2D case it was found by Harris and Kirkpatrick,[30] and more recently in Ref. 37, using a perturbative (linear in x) approach, that the spin-wave self-energy at long wavelengths acquires a nonhydrodynamic contribution which explicitly violates the Lorentz invariance of the clean system (a feature anticipated by Chakravarty *et al.* in Ref. 1). Recently, similar results were obtained in random-phase-approximation studies of a diluted 2D Hubbard model.[5] Some of these studies concluded that $D=2$ is the lower critical dimension for this type of disorder,[30,37] implying an instability of the long-range order to an infinitesimal doping in the Imry-Ma sense.[38] However, as we mentioned above, MC results show that the order is preserved up to $x=x_p$, in contradiction with these conclusions. We will show that the conjecture of the instability is an artifact of a perturbative expansion, and is avoided when the divergent series of diagrams is summed. However, the resulting modification of the excitation spectrum is very unusual, and leads to a number of observable anomalies.

Technically, our approach is similar to one of Brenig and Kampf,[15] who studied the problem of excitation spectrum in diluted 2D QAF's using spin-wave and T-matrix formalisms. However, while the authors of Ref. 15 notes unusually broad peaks in the spectrum, they *assumed* a ''normal'' 3D type of the spectrum renormalization, that is, a softening of the sound velocity and a recovery of the spectrum at long wavelength. The derivative of the spin-wave velocity with x, obtained numerically in Ref. 15 using this assumption, is rather large, $d[c(x)/c_0]/dx \approx -3$, which supported earlier experimental expectations of a QCP at $x<x_p$. A recent work by two of us using a nonlinear σ model allied to classical percolation theory[39] gave a similar result. Another study in Ref. 40 used a generalizations of the σ model with parameters modified according to MC data, and suggested a simple renormalization of spin stiffness $\rho_s(x)$ and spin-wave velocity $c(x)$ as the only effect of impurities. We will show that these results are not correct because of the existence of localized spin excitations which are not taken into account in these works.

In this work we study the problem of impurities in 2D QHAF's within a linear spin-wave theory, using a T-matrix approach combined with a configurational average over the random positions of impurities. We solve the single-impurity problem exactly. The spin-wave Green's function is evaluated by summing all multiple-scattering diagrams that involve a single impurity. This approximation gives results that go beyond a simple linear expansion in x, although not all higher-order contributions in x are taken into account. This approach is valid as long as single-impurity scattering is the dominant one. We recover the results of Refs. 30 and 37 at $k \gg l^{-1}$, that is, the spin-wave spectrum acquires a nonlinear logarithmic contribution $\Sigma_{\mathbf{k}}(\omega) \propto x\, k \ln|\omega|$ with an abnormal damping $\Gamma_{\mathbf{k}} \propto x\, k$. This means that an effective spin-wave velocity $c(x)$ is not well defined. However, we show that there is no instability of the system toward a disordered phase, as conjectured previously. Static properties such as staggered magnetization and the Néel temperature do not possess anomalies, in contrast with the dynamic properties. It is interesting to note that the spin-wave stiffness $\rho_s(x) = c(x)^2 \chi_\perp(x)$ is also well defined, since the anomalous terms in the transverse susceptibility $\chi_\perp(x)$ and in $c(x)$ cancel each other.

We show that a diluted 2D AF provides an example of a system where the arguments for the spectrum to be ''protected'' at long wavelengths fail.[41,42] We have found that the spectrum of a 2D AF at long wavelengths is overdamped at arbitrary concentrations of spinless impurities. More explicitly, the spectrum ceases to contain a quasiparticle peak of any kind beyond a certain length scale. The actual spin excitations, instead of being described as ballistic, may be interpreted as diffusive spin modes. The reason for this is the influence of scattering centers on the long-wavelength excitation, which is not vanishing in two dimensions because of the small phase space. This leads to the absence of an effective self-averaging of the system to a translationally invariant medium with renormalized parameters, as would be the case in three dimensions. Instead, the scattering leads to a length scale $l/a \sim e^{\pi/4x}$ beyond which the influence of impurities on the spectrum is dominant. We associate this length scale with the localization length of spin excitations.

We show that the dynamical structure factor $\mathcal{S}(\mathbf{k},\omega)$, for $a^{-1} \gg k \gg l^{-1}$, consists of three parts (we use units such that $\hbar = k_B = 1$): (i) a broadened quasiparticle peak at an energy $\omega \simeq c_0 k\,(1 + 2x \ln(ka)/\pi)$, where $c_0 = 2\sqrt{2} SJa$ is the bare spin-wave velocity, J is the antiferromagnetic exchange constant, and the width is given by $\Gamma_k \simeq x\, c_0 k$; (ii) a non-Lorentian localization peak at $\omega = \omega_0 \sim c_0 l^{-1}$, and (iii) a flat background of states between $\omega = c_0 k$ and $\omega = \omega_0$. Thus, besides the lack of Lorentz invariance, for every $\mathbf{k}$ state some weight is spread from high energies $\omega \sim c_0 k$ to low energies down to $\omega \sim \omega_0$.[43] For $k \lesssim l^{-1}$ the quasiparticle and localization peaks in $\mathcal{S}(\mathbf{k},\omega)$ merge into a broad incoherent peak that disperses in momentum space.

The anomalies in the dynamical structure factor are reflected in the magnon density of states $N(\omega)$. In a clean 2D AF, $N(\omega) \propto \omega$. With doping $N(\omega)$ acquires a constant contribution from the localized states $N(\omega) \propto \omega + \text{const}\ x$ at $\omega \gg \omega_0$, has a peak at $\omega \approx \omega_0$ of height $\sim 1/x$, and vanishes as $N \propto 1/(x \ln|\omega|)^2$ for $\omega \ll \omega_0$. This behavior of $N(\omega)$ is reminiscent of the problem of localization of Dirac fermions in 2D d-wave superconductors[44] in the case of ''strong'' disorder (unitary scatterers). Another interesting similarity between that problem and an impure 2D AF is that disorder may lead

to very different physical consequences depending on its ''class.'' As noted in Ref. 37 and also in Ref. 45 in another context, one obtains drastically different results if the spin of an impurity is equal to the spin of the host material, and only bond strengths around an impurity (J) are modified. The renormalization of the spectrum in this case does not contain any anomalous terms, namely, $\Sigma_{\mathbf{k}}(\omega) \sim x\, c_0 k$ and $\Gamma_{\mathbf{k}} \sim x\, c_0 k^3 a^2$. According to the terminology of 2D Dirac fermions, this problem falls into the class of a ''weak'' disorder. In the case of spinless impurities the similarity to ''strong'' unitary scattering centers is evident, since no spin degrees of freedom exist at the impurity site.

From the density of states $N(\omega)$ we calculate the magnetic specific heat, which for a clean 2D system at low temperatures is $C_M(0,T) \propto T^2$. We predict a strong deviation from this behavior due to localized states. We find that the specific heat acquires a quasilinear correction $\delta C_M(x,T) = \beta(x) T/(\ln^2|T/\omega_0| + \pi^2/4)$ which is roughly $\propto xT$ at $T \gg \omega_0$. Observation of such a behavior can provide a simple test of our theory. We remark that in our approach the contribution of the finite (decoupled) clusters is not taken into account, since the whole system is considered as a single, ordered, infinite cluster. However, finite clusters of size L have a gap in their spectrum of order J/L, and thus become important in the low-T region only at x close to percolation threshold where L can be large. Another source of similar high-energy corrections is due to the resonant states ($\omega_{res} \sim J$), around impurities whose energy may go down with doping.[46] At lower temperatures $T \lesssim \sqrt{J_\perp J}$, where $J_\perp$ is the interplane exchange constant, a crossover to a 3D behavior should be seen. Thus, for x not too close to x_p, we expect a large temperature window where the predicted anomalous 2D behavior of C_M in the infinite cluster is dominant and can be observed.

We also consider the effects of small interplane coupling $\tau_{3D} = J_\perp/2J$ and small anisotropy gaps on our conclusions for dynamical properties of a strictly 2D isotropic AF discussed above. It is evident that as long as these additional energy scales are small in comparison with J, there will be an energy range $1 \gg \omega/J \gg \sqrt{\tau}$ ($\tau = \tau_{eff}$ accumulating the total effect of the gaps and 3D coupling) in which the nonlinearity of the spectrum and an abnormal damping of the 2D spin waves should be observable. A more delicate question is if the localization part of the spectrum and truly overdamped long-wavelength excitations can be seen in the presence of gaps or 3D coupling. The point is that the disorder induced scale $\omega_0 \sim J e^{-\pi/4x}$ can be hindered by these additional terms, which cut off the log singularity. Therefore, a range of concentrations $0 < x < x^* \sim \ln^{-1}(1/\tau)$ can be found where the long-wavelength quasiparticles are still well defined deep in the 3D region of the $\mathbf{k}$ space ($ka \ll \sqrt{\tau}$), similar to the quasi-1D problem.[47] For LCO materials, $\tau \sim 10^{-4}$ gives $x^* \sim 0.1$–0.2. Above concentration x^* (and at $x < x_p$), localization and overdamped peaks should be observable since $\omega_0 > \sqrt{\tau}$, and all the low-energy excitations become incoherent. Our order of magnitude estimation for the largest value of τ which can allow such observation (from the condition $x^* < x_p$) is $\tau \sim 0.01$. Therefore, a rather high impurity concentration and small enough anisotropies and inter planar coupling may be required to observe directly some of the dynamical effects we predict in this work.

We calculate the static magnetic properties and find a quantitative agreement with both MC simulations and experimental data. We show that at $T=0$ the staggered magnetization (averaged over the magnetic sites[48]) is given by $M(x,0) \approx S - \Delta - Bx$ for $x \ll 1$; the factor $\Delta = \Sigma_k v_{\mathbf{k}}^2 \approx 0.2$ stands for the contribution of the zero-point fluctuations of the spins, and $B \simeq 0.21$ is S independent in our approach. We find that $T_N(x)/T_N(0) \simeq 1 - A_s x$ for $x \ll 1$, where $A_s = \pi - 2/\pi + B/(S-\Delta)$ is a weak function of S. This linear expansion result gives $A_{1/2} \simeq 3.2$ and $A_{5/2} \simeq 2.6$, which work quite well up to a high value of $x \sim 0.25$. It is interesting that the linear expansion results point to $x_c(1/2) \simeq 0.31$ and $x_c(5/2) \simeq 0.38$, both below x_p, which means that $T_N(x)$ versus x curve should be concave, in contrast with the 2D Ising magnets for which $T_N(x)$ is a more traditional convex curve.[17] Such an anomalous curvature of the ordering temperature was also observed in many different magnetic systems composed of f-electron moments such as U and Ce.[49] We show that in our approach for larger values of $xT_N(x)$ indeed bends inward, and tends to saturate close to x_p. We interpret this behavior as due to localization effects which tend to reduce the role of quantum fluctuations in the destruction of the long-range order.

We have calculated the 2D magnetic correlation length $\xi(x,T)$, to describe the paramagnetic phase of the system above the Néel temperature. We used a modified spin-wave theory formalism of Takahashi,[50] and calculated $\xi(x,T)$ numerically. The correlation length is suppressed in comparison with the pure case, and also shows some deviation from a simple $e^{2\pi\rho_s(x)/T}$ behavior at larger x.

This paper is organized as follows: we describe the model and introduce the formalism in Sec. II. In Sec. III we present results for the dynamic properties. In Sec. IV, the static properties and long-range order and discussed; Section V contains our conclusions. A few appendixes are included with details of the calculations. Some of the results presented here were briefly reported in our previous paper.[51]

II. FORMALISM

The systems discussed in this paper are modeled by the site-diluted quantum Heisenberg antiferromagnet

$$H = \sum_{\langle ij \rangle} J_{ij}\, p_i\, p_j\, \mathbf{S}_i \cdot \mathbf{S}_j, \tag{1}$$

where $p_i = 1$ (0) if the $\mathbf{R}_i$ site is occupied (unoccupied) by the spin S. We focus on the problem of tetragonal or square lattices with in-plane, J, and out-of-plane, $J_\perp$, nearest-neighbor exchange constants; $\langle ij \rangle$ denotes a summation over bonds. In the systems of interest $J \gg J_\perp$ (for instance, in LCO $J \approx 1500$ K and $J_\perp \sim 10^{-4} J$).

A. Spin-wave approximation

We begin with Hamiltonian (1) which is split into the pure host and impurity parts,

$$\mathcal{H}=\mathcal{H}_0+\mathcal{H}_{imp}=\sum_{\langle ij\rangle} J_{ij}\,\mathbf{S}_i\cdot\mathbf{S}_j-\sum_{l,\delta} J_{l,\delta}\mathbf{S}_l\cdot\mathbf{S}_{l+\delta}, \quad (2)$$

where l runs over the impurity sites and δ is a nearest-neighbor unity vector. Then, in the linear spin-wave approximation,

$$S_i^z=S-a_i^\dagger a_i, \quad S_i^+\simeq\sqrt{2S}a_i, \quad S_i^-\simeq\sqrt{2S}a_i^\dagger, \quad (3)$$

$$S_j^z=-S+b_j^\dagger b_j, \quad S_j^+\simeq\sqrt{2S}b_j^\dagger, \quad S_j^-\simeq\sqrt{2S}b_j,$$

for spins in A (i) and B (j) sublattices, the quadratic part of the pure host Hamiltonian $\mathcal{H}_0$ for the tetragonal lattice is given by

$$\mathcal{H}_0=4SJ\sum_{\mathbf{k}}\,[\,\hat{\gamma}_0(a_\mathbf{k}^\dagger a_\mathbf{k}+b_\mathbf{k}^\dagger b_\mathbf{k})+\hat{\gamma}_\mathbf{k}(a_\mathbf{k}^\dagger b_{-\mathbf{k}}^\dagger+b_{-\mathbf{k}}a_\mathbf{k})\,], \quad (4)$$

where in-plane and out-of-plane coordination numbers are $z=4$ and $z_\perp=2$, respectively, and we define

$$\hat{\gamma}_\mathbf{k}=\gamma_\mathbf{k}+\tau\gamma_\mathbf{k}^\perp, \quad (5)$$

with $\tau=J_\perp/2J$, $\gamma_\mathbf{k}=(\cos k_x+\cos k_y)/2$, and $\gamma_\mathbf{k}^\perp=\cos k_z$. From now on the in-plane and out-of-plane momenta are in units of the correspondent inverse lattice constants. The impurity parts of Hamiltonian (2) on a tetragonal lattice are

$$\mathcal{H}_{imp}^A=-S\sum_{l\in A,\delta} J_{l,\delta}[a_l^\dagger a_l+b_{l+\delta}^\dagger b_{l+\delta}+a_l^\dagger b_{l+\delta}^\dagger+a_l b_{l+\delta}], \quad (6)$$

$$\mathcal{H}_{imp}^B=\mathcal{H}_{imp}^A(a\leftrightarrow b),$$

with $J_{l,\delta}=J$ ($J_\perp$) for $\delta=e_x,e_y$ (e_z). After Fourier transformation it is more convenient to write the impurity Hamiltonian in 2×2 matrix notations,

$$\mathcal{H}_{imp}=-4SJ\sum_{l,\mathbf{k},\mathbf{k}'} e^{i(\mathbf{k}-\mathbf{k}')\mathbf{R}_l}\hat{A}_\mathbf{k}^\dagger\hat{V}_{\mathbf{k},\mathbf{k}'}^l\hat{A}_{\mathbf{k}'}, \quad (7)$$

where

$$\hat{A}_\mathbf{k}=\begin{bmatrix} a_\mathbf{k} \\ b_{-\mathbf{k}}^\dagger \end{bmatrix}, \quad \hat{A}_\mathbf{k}^\dagger=[a_\mathbf{k}^\dagger,\ b_{-\mathbf{k}}], \quad (8)$$

with scattering potentials for l in the sublattice A,

$$\hat{V}_{\mathbf{k},\mathbf{k}'}^A=\begin{pmatrix} \hat{\gamma}_0 & \hat{\gamma}_{\mathbf{k}'} \\ \hat{\gamma}_\mathbf{k} & \hat{\gamma}_{\mathbf{k}-\mathbf{k}'} \end{pmatrix}, \quad (9)$$

and for l in the sublattice B:

$$\hat{V}_{\mathbf{k},\mathbf{k}'}^B=\begin{pmatrix} \hat{\gamma}_{\mathbf{k}-\mathbf{k}'} & \hat{\gamma}_\mathbf{k} \\ \hat{\gamma}_{\mathbf{k}'} & \hat{\gamma}_0 \end{pmatrix}. \quad (10)$$

The pure host Hamiltonian [Eq. (4)] is diagonalized using Bogolyubov transformations

$$a_\mathbf{k}=u_\mathbf{k}\alpha_\mathbf{k}+v_\mathbf{k}\beta_{-\mathbf{k}}^\dagger, \quad (11)$$

$$b_\mathbf{k}^\dagger=u_\mathbf{k}\beta_\mathbf{k}^\dagger+v_\mathbf{k}\alpha_{-\mathbf{k}},$$

with

$$u_\mathbf{k}^2-v_\mathbf{k}^2=1, \quad 2u_\mathbf{k}v_\mathbf{k}=-\hat{\gamma}_\mathbf{k}/\omega_\mathbf{k}, \quad (12)$$

$$u_\mathbf{k}=\sqrt{\frac{\hat{\gamma}_0+\omega_\mathbf{k}}{2\omega_\mathbf{k}}}, \quad v_\mathbf{k}=-\,\mathrm{sgn}\,\hat{\gamma}_\mathbf{k}\sqrt{\frac{\hat{\gamma}_0-\omega_\mathbf{k}}{2\omega_\mathbf{k}}},$$

where the bare spin-wave frequency is

$$\omega_\mathbf{k}=\sqrt{\hat{\gamma}_0^2-\hat{\gamma}_\mathbf{k}^2}. \quad (13)$$

The problem can be reduced to the problem in a 2D square lattice by letting $\tau\to0$ in Eqs. (4)–(13). In what follows all energies are expressed in units of $\Omega_0=4SJ$.

After the Bogolyubov transformation the Hamiltonian Equations (4) and (7) are given by (in the units of Ω_0)

$$\mathcal{H}_0=\sum_\mathbf{k}\ \omega_\mathbf{k}(\alpha_\mathbf{k}^\dagger\alpha_\mathbf{k}+\beta_\mathbf{k}^\dagger\beta_\mathbf{k}), \quad (14)$$

$$\mathcal{H}_{imp}=-\sum_{l,\mathbf{k},\mathbf{k}'} e^{i(\mathbf{k}-\mathbf{k}')\mathbf{R}_l}\hat{\mathcal{A}}_\mathbf{k}^\dagger\hat{\mathcal{V}}_{\mathbf{k},\mathbf{k}'}^l\hat{\mathcal{A}}_{\mathbf{k}'}, \quad (15)$$

where the two-component vectors are

$$\hat{\mathcal{A}}_\mathbf{k}=\begin{bmatrix} \alpha_\mathbf{k} \\ \beta_{-\mathbf{k}}^\dagger \end{bmatrix}, \quad \hat{\mathcal{A}}_\mathbf{k}^\dagger=[\alpha_\mathbf{k}^\dagger,\ \beta_{-\mathbf{k}}], \quad (16)$$

and 2×2 scattering potential matrices $\hat{\mathcal{V}}_{\mathbf{k},\mathbf{k}'}$ are obtained from Eqs. (9) and (10) using Eq. (11). For the sake of further use of the T-matrix formalism, it is convenient to decompose the scattering potentials into orthogonal components according to the symmetry with respect to the scattering site. The symmetry of the tetragonal lattice is D_{4h}, which is a group of order 16 and has ten irreducible representations. Since the impurity potentials [Eqs. (9 and 10)] connect only nearest-neighbor sites, only five components of the scattering potentials in irreducible representations of D_{4h} are nonzero. They correspond to the irreducible representations A_{1g}, B_{1g}, B_{2g}, and E_u. These nonzero components are the s wave, the in-plane p_x, p_y, and d waves, and the out-of-plane p_z wave (for details see Appendix A).

Thus, the scattering potential for the impurity in the sublattice A

$$\hat{\mathcal{V}}_{\mathbf{k},\mathbf{k}'}^A=\sum_\mu\ \hat{\mathcal{V}}_{\mathbf{k},\mathbf{k}'}^{A,\mu}, \quad (17)$$

where the scattering channels are $\mu=s,p_x,p_y,d,p_z$. In each channel the scattering potentials can be written as a direct product of the column and row vectors. The s-wave part is

$$\hat{\mathcal{V}}_{\mathbf{k},\mathbf{k}'}^{A,s}=|s_\mathbf{k}\rangle\otimes\langle s_{\mathbf{k}'}|+\tau|s_\mathbf{k}^\perp\rangle\otimes\langle s_{\mathbf{k}'}^\perp|, \quad (18)$$

where

$$\langle s_\mathbf{k}|=[u_\mathbf{k}+v_\mathbf{k}\gamma_\mathbf{k},\ v_\mathbf{k}+u_\mathbf{k}\gamma_\mathbf{k}],$$

and

$$\langle s_\mathbf{k}^\perp|=[u_\mathbf{k}+v_\mathbf{k}\gamma_\mathbf{k}^\perp,\ v_\mathbf{k}+u_\mathbf{k}\gamma_\mathbf{k}^\perp],$$

the in-plane p-wave part is

$$\hat{\mathcal{V}}^{A,p_{x(y)}}_{\mathbf{k},\mathbf{k}'}=|p^{x(y)}_{\mathbf{k}}\rangle\otimes\langle p^{x(y)}_{\mathbf{k}'}|, \tag{19}$$

where

$$\langle p^{x(y)}_{\mathbf{k}}|=\sin k_{x(y)}[v_{\mathbf{k}},\ u_{\mathbf{k}}]/\sqrt{2},$$

the d-wave part is

$$\hat{\mathcal{V}}^{A,d}_{\mathbf{k},\mathbf{k}'}=|d_{\mathbf{k}}\rangle\otimes\langle d_{\mathbf{k}'}|, \tag{20}$$

where

$$\langle d_{\mathbf{k}}|=\gamma^{-}_{\mathbf{k}}[v_{\mathbf{k}},\ u_{\mathbf{k}}],$$

with

$$\gamma^{-}_{\mathbf{k}}=(\cos k_x-\cos k_y)/2,$$

and the out-of-plane p_z-wave contribution is

$$\hat{\mathcal{V}}^{A,p_z}_{\mathbf{k},\mathbf{k}'}=\tau|p^{z}_{\mathbf{k}}\rangle\otimes\langle p^{z}_{\mathbf{k}'}|, \tag{21}$$

where

$$\langle p^{z}_{\mathbf{k}}|=\sin k_z[v_{\mathbf{k}},\ u_{\mathbf{k}}]/\sqrt{2}.$$

For the impurity in B sublattice, $\hat{\mathcal{V}}^{B,\mu}_{\mathbf{k},\mathbf{k}'}\equiv\hat{\mathcal{V}}^{A,\mu}_{\mathbf{k},\mathbf{k}'}(u\leftrightarrow v)$.

In what follows we consider the 2D ($\tau=0$) or quasi-2D ($\tau\ll 1$) limit of the problem. It can be shown that the contribution of the out-of-plane terms in s- and p_z-wave scattering potentials which explicitly depend on τ, as well as the one of the majority of the τ-dependent terms originating from the quasi-2D form of $u_{\mathbf{k}}$, $v_{\mathbf{k}}$, and $\omega_{\mathbf{k}}$ [Eqs. (12) and (13)], is negligible in the quasi-2D case [$\sim O(\tau)$, see Appendix B]. This allows one to simplify the scattering problem further by neglecting the $s^{\perp}$ and p_z components in the above equations. Moreover, the solution for the 2D problem can be applied directly to the quasi-2D case, since the formal expressions are identical in both cases. The only important difference concerns the logarithmically divergent terms, which in a quasi-2D system acquire a low-energy cutoff provided by the implicit dependence of scattering potentials (19)–(22) on τ through $\omega_{\mathbf{k}}$. This simply means that, for the quasi-2D case in the limit $\tau\ll 1$, one can restrict oneself by considering purely 2D scattering including the three-dimensionality only on the level of the spin-wave dispersion in certain terms. Thus in the following we use

$$\hat{\mathcal{V}}^{A,s}_{\mathbf{k},\mathbf{k}'}=|s_{\mathbf{k}}\rangle\otimes\langle s_{\mathbf{k}'}|,$$
$$\text{with}\ \ \langle s_{\mathbf{k}}|=\omega_{\mathbf{k}}[u_{\mathbf{k}},\ -v_{\mathbf{k}}]. \tag{22}$$

The rest of this section is devoted to the 2D limit of the problem and, unless specified otherwise, we use

$$\hat{\gamma}_{\mathbf{k}}=\gamma_{\mathbf{k}}=(\cos k_x+\cos k_y)/2,$$
$$\hat{\gamma}_0=1,\quad \omega_{\mathbf{k}}=\sqrt{1-\gamma^2_{\mathbf{k}}}. \tag{23}$$

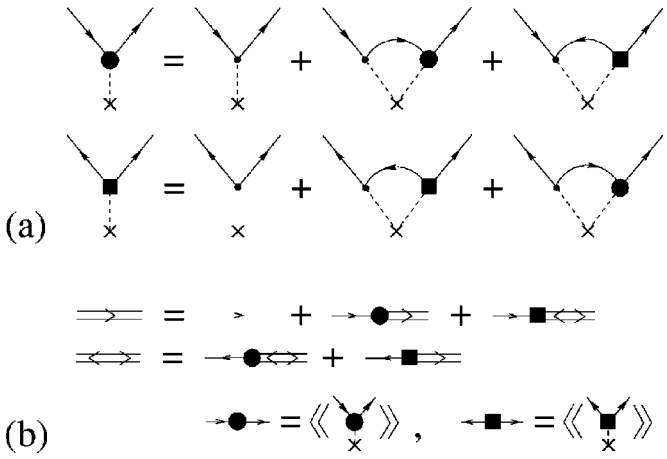

FIG. 1. (a) T-matrix single-impurity scattering series (b) Dyson-Belyaev diagram series for the diagonal, G^{11}, and off-diagonal, G^{12}, Green's functions. The self-energies Σ^{11} (circle) and Σ^{12} (square) are the configurational averages of T^{11} and T^{12} components of the T matrix, respectively.

B. *T*-matrix. Single-impurity scattering

We are interested in the Green's function of Hamiltonian (14) modified by random impurity potentials [Eqs. (15)]. The Green's function is a 2×2 matrix defined in a standard way,

$$\begin{aligned}
G^{11}_{\mathbf{k}}(t)&=-i\langle T[\alpha_{\mathbf{k}}(t)\alpha^{\dagger}_{\mathbf{k}}(0)]\rangle,\\
G^{12}_{\mathbf{k}}(t)&=-i\langle T[\alpha_{\mathbf{k}}(t)\beta_{-\mathbf{k}}(0)]\rangle,\\
G^{21}_{\mathbf{k}}(t)&=-i\langle T[\beta^{\dagger}_{-\mathbf{k}}(t)\alpha^{\dagger}_{\mathbf{k}}(0)]\rangle,\\
G^{22}_{\mathbf{k}}(t)&=-i\langle T[\beta^{\dagger}_{\mathbf{k}}(t)\beta_{\mathbf{k}}(0)]\rangle,
\end{aligned} \tag{24}$$

where brackets also imply a configurational average over the impurity sites.

The T-matrix equation for Hamiltonian (15) is given by

$$\hat{T}^{l,\mu}_{\mathbf{k},\mathbf{k}'}(\omega)=-\hat{\mathcal{V}}^{l,\mu}_{\mathbf{k},\mathbf{k}'}-\sum_{\mathbf{q}}\ \hat{\mathcal{V}}^{l,\mu}_{\mathbf{k},\mathbf{q}}\hat{G}^{0}_{\mathbf{q}}(\omega)\hat{T}^{l,\mu}_{\mathbf{q},\mathbf{k}'}(\omega), \tag{25}$$

with $l=A(B)$; partial waves are restricted to in-plane $\mu=s,p_{\sigma},d$ harmonics according to the above discussion, and $\hat{G}^{0}_{\mathbf{q}}(\omega)$ is the 2×2 bare Green's function:

$$G^{0,11}_{\mathbf{q}}(\omega)=G^{0,22}_{\mathbf{q}}(-\omega)=\frac{1}{\omega-\omega_{\mathbf{q}}+i0},$$
$$G^{0,12}_{\mathbf{q}}(\omega)=G^{0,21}_{\mathbf{q}}(\omega)=0. \tag{26}$$

The diagrammatic equivalent of Eq. (25) is shown in Fig. 1(a). T-matrix equations (25) with potentials (19)–(22), can be readily solved:

$$\hat{T}^{A,\mu}_{\mathbf{k},\mathbf{k}'}(\omega)=\hat{\mathcal{V}}^{A,\mu}_{\mathbf{k},\mathbf{k}'}\Gamma_{\mu}(\omega),$$
$$\hat{T}^{B,\mu}_{\mathbf{k},\mathbf{k}'}(\omega)=\hat{\mathcal{V}}^{B,\mu}_{\mathbf{k},\mathbf{k}'}\Gamma_{\mu}(-\omega), \tag{27}$$

where the frequency-dependent parts are given by

$$\Gamma_s(\omega)=\frac{1}{\omega}+\frac{(1+\omega)\rho(\omega)}{1-\omega(1+\omega)\rho(\omega)}, \tag{28}$$

$$\Gamma_p(\omega) = -\frac{2}{1+\omega+(1-\omega)[\omega^2\rho(\omega)-\rho_d(\omega)]},$$

$$\Gamma_d(\omega) = -\frac{1}{1+(1-\omega)\rho_d(\omega)},$$

with

$$\rho(\omega) = \sum_{\mathbf{p}} \frac{1}{\omega^2-\omega_{\mathbf{p}}^2}, \quad \rho_d(\omega) = \sum_{\mathbf{p}} \frac{(\gamma_{\mathbf{p}}^-)^2}{\omega^2-\omega_{\mathbf{p}}^2}. \tag{29}$$

We note here that the second term in this s wave $\Gamma_s(\omega)$ is proportional to $\rho(\omega)$ at $\omega \ll 1$, where the latter appears naturally from the summation in Fig. 1(a) as the result of a combination of $G_{\mathbf{q}}^{0,11}(\omega)$ and $G_{\mathbf{q}}^{0,22}(\omega)$ in the internal part of the diagrams. When the summation over $\mathbf{p}$ in Eq. (29) is restricted to two dimensions $\rho(\omega)$ is a logarithmic function at low energies. In the following we show that this contribution to the s-wave scattering is solely responsible for all the anomalies in the spectrum of a 2D AF. Interestingly, a similar logarithmic term in the self-energy of the 2D Dirac fermions in the problem of disorder in d-wave superconductors requires a summation of the specific subset of diagrams.[52] In our case, while one needs to sum infinite series of diagrams, no special selection or inclusion of the multiple-impurity scattering processes is necessary. Since the single-particle density of states and the sensitivity of the results to the type of disorder in both problems are similar, establishing a detailed correspondence between these two problems is an important question. Integrals in Eq. (29) can be taken analytically and, in a 2D case, are expressed through the complete elliptic integrals[15] (see Appendix C).

The first term in the s-wave scattering [Eq. (28)] represents a singular zero-frequency mode which is independent of the dimension of the problem, and originates from oscillations of the fictitious spin degrees of freedom at the impurity site which are decoupled from the AF matrix. Roughly speaking, when the spins are quantized as in Eq. (3), and S' at the impurity site is set to zero, there is still $a_0^\dagger a_0$ left from S_0^z. Thus, in the spin-wave approximation, it gives rise to an s-wave zero-frequency mode. This problem has been noted since the earliest works on the diluted magnets which used the spin-wave theory,[31] and also more recently in the context of a diluted AF (Refs. 7,15,37,45 and 53) (for an extensive discussion, see Ref. 37). Since these states are unphysical and are unrelated to the low-energy physics of the AF, they have to be projected out. One of the projection schemes involves a non-Hermitian potential which was designed to preserve the simplest factorized form of the s-wave scattering potential.[37] We use another, physically more transparent scheme which introduces a fictitious magnetic fields at the impurity sites (similar to Refs. 15 and 45),

$$\Delta\mathcal{H} = H_z \sum_l a_l^\dagger a_l \Rightarrow H_z \sum_{l,\mathbf{k},\mathbf{k}'} e^{i(\mathbf{k}-\mathbf{k}')\mathbf{R}_l} \hat{\mathcal{A}}_{\mathbf{k}}^\dagger \Delta\hat{\mathcal{V}}_{\mathbf{k},\mathbf{k}'}^{l,s} \hat{\mathcal{A}}_{\mathbf{k}'}, \tag{30}$$

where corrections to the s-wave scattering potential are

$$\Delta\hat{\mathcal{V}}_{\mathbf{k},\mathbf{k}'}^{A,s} = |\Delta s_{\mathbf{k}}\rangle \otimes \langle \Delta s_{\mathbf{k}'}|,$$

with

$$\langle \Delta s_{\mathbf{k}}| = [u_{\mathbf{k}}, \ v_{\mathbf{k}}], \tag{31}$$

$\Delta\hat{\mathcal{V}}_{\mathbf{k},\mathbf{k}'}^{B,s} = \Delta\hat{\mathcal{V}}_{\mathbf{k},\mathbf{k}'}^{A,s}\{u \leftrightarrow v\}$. Evidently, p and d waves are not affected by the projection. Within our approach, after some algebra in the limit $H_z \to \infty$, one obtains a modified T-matrix solution (for the case of an arbitrary H_z see Appendix D),

$$\hat{T}_{\mathbf{k},\mathbf{k}'}^{A,s}(\omega) = \hat{\mathcal{V}}_{\mathbf{k},\mathbf{k}'}^{A,s}\Gamma_s(\omega) + \Delta\hat{T}_{\mathbf{k},\mathbf{k}'}^{A,s}(\omega), \tag{32}$$

$$\hat{T}_{\mathbf{k},\mathbf{k}'}^{B,s}(\omega) = \hat{\mathcal{V}}_{\mathbf{k},\mathbf{k}'}^{B,s}\Gamma_s(-\omega) + \Delta\hat{T}_{\mathbf{k},\mathbf{k}'}^{B,s}(\omega),$$

where $\hat{\mathcal{V}}_{\mathbf{k},\mathbf{k}'}^{l,s}$ is given, as before, by Eq. (18) and the frequency-dependent part is now free from the zero-frequency pole

$$\Gamma_s(\omega) = \frac{(1+\omega)\rho(\omega)}{1-\omega(1+\omega)\rho(\omega)}. \tag{33}$$

Comparing this expression with Eq. (28), one may note that the ''physical'' term is left unchanged after the projection. Additional terms in solution (32) are also regular:

$$\Delta\hat{T}_{\mathbf{k},\mathbf{k}'}^{A,s}(\omega) = -\omega|\Delta s_{\mathbf{k}}\rangle \otimes \langle \Delta s_{\mathbf{k}'}| + |s_{\mathbf{k}}\rangle \otimes \langle \Delta s_{\mathbf{k}'}| + |\Delta s_{\mathbf{k}}\rangle \otimes \langle s_{\mathbf{k}'}|, \tag{34}$$

with $|s_{\mathbf{k}}\rangle$ from Eq. (22) and $|\Delta s_{\mathbf{k}}\rangle$ from Eq. (31); $\hat{T}_{\mathbf{k},\mathbf{k}'}^{B,s}(\omega) = \hat{T}_{\mathbf{k},\mathbf{k}'}^{A,s}(-\omega)\{u \leftrightarrow v\}$, as before. Thus, projection (30) allows one to remove the unphysical divergency at $\omega = 0$ which would otherwise affect the true low-energy physics of the problem.

C. Green's function

The averaging over random distribution of impurities readily transforms the T matrix into spin-wave self-energies,

$$\hat{\Sigma}_{\mathbf{k}}(\omega) = \sum_{\mu} \hat{\Sigma}_{\mu,\mathbf{k}}(\omega), \tag{35}$$

with μ-wave contributions

$$\hat{\Sigma}_{\mu,\mathbf{k}}(\omega) = x\,\delta_{\mathbf{k}-\mathbf{k}'}[\hat{T}_{\mathbf{k},\mathbf{k}'}^{A,\mu}(\omega) + \hat{T}_{\mathbf{k},\mathbf{k}'}^{B,\mu}(\omega)]. \tag{36}$$

For the 2D case the contributions of the partial waves to the self-energies are

$$\hat{\Sigma}_{s,\mathbf{k}}(\omega) = x\omega_{\mathbf{k}}\left[\begin{pmatrix} 1 & \gamma_{\mathbf{k}} \\ \gamma_{\mathbf{k}} & 1 \end{pmatrix}\frac{\Gamma_s(\omega)+\Gamma_s(-\omega)}{2} + \begin{pmatrix} \omega_{\mathbf{k}} & 0 \\ 0 & -\omega_{\mathbf{k}} \end{pmatrix}\frac{\Gamma_s(\omega)-\Gamma_s(-\omega)}{2} - \begin{pmatrix} 2 & 0 \\ 0 & 2 \end{pmatrix}\right] - x\omega\begin{pmatrix} 1 & 0 \\ 0 & -1 \end{pmatrix}, \tag{37}$$

$$\hat{\Sigma}_{p,\mathbf{k}}(\omega)=x\omega_{\mathbf{k}}\left[1-\left(\frac{\gamma_{\mathbf{k}}^{-}}{\omega_{\mathbf{k}}}\right)^2\right]\left[\begin{pmatrix}1 & -\gamma_{\mathbf{k}}\\ -\gamma_{\mathbf{k}} & 1\end{pmatrix}\frac{\Gamma_p(\omega)+\Gamma_p(-\omega)}{2}+\begin{pmatrix}-\omega_{\mathbf{k}} & 0\\ 0 & \omega_{\mathbf{k}}\end{pmatrix}\frac{\Gamma_p(\omega)-\Gamma_p(-\omega)}{2}\right], \tag{38}$$

$$\hat{\Sigma}_{d,\mathbf{k}}(\omega)=x\omega_{\mathbf{k}}\left(\frac{\gamma_{\mathbf{k}}^{-}}{\omega_{\mathbf{k}}}\right)^2\left[\begin{pmatrix}1 & -\gamma_{\mathbf{k}}\\ -\gamma_{\mathbf{k}} & 1\end{pmatrix}\frac{\Gamma_d(\omega)+\Gamma_d(-\omega)}{2}+\begin{pmatrix}-\omega_{\mathbf{k}} & 0\\ 0 & \omega_{\mathbf{k}}\end{pmatrix}\frac{\Gamma_d(\omega)-\Gamma_d(-\omega)}{2}\right]. \tag{39}$$

It is interesting to observe that ''on-shell'' (at $\omega=\omega_{\mathbf{k}}$) ''projected'' $\hat{T}^{s}_{\mathbf{k},\mathbf{k}'}(\omega)$ from Eqs. (32)–(34) and ''nonprojected'' expressions [Eq. (27), and (28)] yield identical $\Sigma_{s,\mathbf{k}}(\omega_{\mathbf{k}})$.

Summation of the Dyson-Belyaev diagrammatic series for the Green's functions shown in Fig. 1(b), with self-energies defined in Eqs. (35)–(39), gives

$$\hat{G}_{\mathbf{k}}(\omega)=\begin{pmatrix}-\omega-\omega_{\mathbf{k}}-\Sigma^{22}_{\mathbf{k}}(\omega) & \Sigma^{12}_{\mathbf{k}}(\omega)\\ \Sigma^{21}_{\mathbf{k}}(\omega) & \omega-\omega_{\mathbf{k}}-\Sigma^{11}_{\mathbf{k}}(\omega)\end{pmatrix}\frac{1}{[\omega-\omega_{\mathbf{k}}-\Sigma^{11}_{\mathbf{k}}(\omega)][-\omega-\omega_{\mathbf{k}}-\Sigma^{22}_{\mathbf{k}}(\omega)]-[\Sigma^{12}_{\mathbf{k}}(\omega)]^2}, \tag{40}$$

where $\Sigma^{22}_{\mathbf{k}}(\omega)=\Sigma^{11}_{\mathbf{k}}(-\omega)$. A detailed consideration of the properties of spectral functions

$$A^{ij}_{\mathbf{k}}(\omega)=-\frac{1}{\pi}\,\mathrm{Im}\,\hat{G}^{ij}_{\mathbf{k}}(\omega), \tag{41}$$

will be given in Sec. III.

We investigate the neutron-scattering dynamical structure factor $\mathcal{S}(\mathbf{k},\omega)$,

$$\mathcal{S}^{\alpha\beta}(\mathbf{k},\omega)=\int_{-\infty}^{\infty}dt\,e^{i\omega t}\langle S^{\alpha}_{\mathbf{k}}(t)S^{\beta}_{-\mathbf{k}}(0)\rangle, \tag{42}$$

which is directly related to the spin Green's functions. The standard derivation of the single-magnon contribution to the transverse component of the dynamical structure factor $\mathcal{S}^{+-}(\mathbf{k},\omega)$ at $T=0$ gives

$$\mathcal{S}^{+-}(\mathbf{k},\omega)=\pi S(u_{\mathbf{k}}+v_{\mathbf{k}})^2[A^{11}_{\mathbf{k}}(\omega)+A^{22}_{\mathbf{k}}(\omega)+2A^{12}_{\mathbf{k}}(\omega)], \tag{43}$$

where the kinematic (ω-independent) form factor $(u_{\mathbf{k}}+v_{\mathbf{k}})^2=(1-\gamma_{\mathbf{k}})/\omega_{\mathbf{k}}$ is proportional to k close to the ''nuclear'' reciprocal-lattice point $\mathbf{K}=0$, and is $\sim 1/k$ close to the ''magnetic'' $\mathbf{Q}=(\pi,\pi)$ point. It thus enhances the signal close to the AF ordering vector, and suppresses it close to the zone center. Note that the diagonal parts of the Green's function are symmetric and off-diagonal parts are asymmetric with respect to the transformation $\mathbf{k}\rightarrow\mathbf{k}+\mathbf{Q}$ (since $G^{12}\sim\Sigma^{12}$ and $\Sigma^{12}_{\mathbf{k}+\mathbf{Q}}=-\Sigma^{12}_{\mathbf{k}}$). Therefore, the sum of the spectral functions in the brackets in Eq. (43) is, generally speaking, different in the magnetic and nuclear parts of the Brillouin zone. At $T>0$, expression (43) is modified by the factor $[1+n_B(\omega)]$, where $n_B(\omega)=[e^{\omega/T}-1]^{-1}$ is the Bose distribution function.

The density of states associated with magnetic excitations is straightforwardly related to the magnon Green's function [Eq. (40)], and is given by

$$N(\omega)=\sum_{\mathbf{k}}\,[A^{11}_{\mathbf{k}}(\omega)+A^{22}_{\mathbf{k}}(\omega)]. \tag{44}$$

The magnetic specific heat is then given by

$$C_M(T)=\frac{1}{T^2}\int_0^1 d\omega\,N(\omega)\omega^2\,[n_B(\omega)^2+n_B(\omega)], \tag{45}$$

where ω and T are in units of $\Omega_0=4SJ$.

The static properties of the system, such as the staggered magnetization in the ordered phase, the Nèel temperature, and the 2D correlation length in the paramagnetic phase, are calculated from the spin-wave expression of the averaged on-site magnetic moment,

$$|\langle S^z_i\rangle|=S-\frac{1}{2}\sum_{\mathbf{k}}\left(\frac{1}{\omega_{\mathbf{k}}}-1\right)-\sum_{\mathbf{k}}\frac{1}{\omega_{\mathbf{k}}}[\langle\alpha^{\dagger}_{\mathbf{k}}\alpha_{\mathbf{k}}\rangle-\gamma_{\mathbf{k}}\langle\alpha^{\dagger}_{\mathbf{k}}\beta^{\dagger}_{\mathbf{k}}\rangle], \tag{46}$$

where bosonic averages can be expressed through spectral functions (41) as

$$\langle\alpha^{\dagger}_{\mathbf{k}}\alpha_{\mathbf{k}}\rangle=\int_{-\infty}^{\infty}d\omega\,n_B(\omega)A^{11}_{R,\mathbf{k}}(\omega), \tag{47}$$

$$\langle\alpha^{\dagger}_{\mathbf{k}}\beta^{\dagger}_{\mathbf{k}}\rangle=\int_{-\infty}^{\infty}d\omega\,n_B(\omega)\,A^{12}_{R,\mathbf{k}}(\omega),$$

which implicitly depend on the impurity concentration x; index R stands for retarded.

In the ordered phase expressions (46), and (47) provide us with the concentration and temperature dependence of the averaged staggered magnetization $M(x,T)$. The same expressions, with the condition $\langle S^z\rangle(x,T)=0$, define the mean-field equation on the Néel temperature as a function of x. In both cases, when $T\neq 0$ the 3D form of the spin-wave dispersion is to be used in Eq. (46). In the paramagnetic phase ($T>T_N$) Eq. (46) should be modified by $\gamma_{\mathbf{k}}\rightarrow\eta\gamma_{\mathbf{k}}$ and $\omega_{\mathbf{k}}\rightarrow\sqrt{1-\eta^2\gamma^2_{\mathbf{k}}}$. Then, in the framework of the modified spin-wave theory,[50] equation $\langle S^z_i\rangle(x,T,\eta)=0$ is a constraint which represents a self-consistent equation on the gap $\sqrt{1-\eta^2}$. This, in turn, defines the 2D correlation length ξ_{2D} as a function of x and T.

III. DYNAMIC AND THERMODYNAMIC PROPERTIES

In this section we consider in detail the structure of the spectral functions of the Green's function [Eq. (40)], Fig. 1(b), with self-energies given by Eqs. (35)–(39). We calculate the dynamical structure factor $\mathcal{S}(\mathbf{k},\omega)$, the spin-wave density of states $N(\omega)$, and the low-T magnetic specific heat $C_M(T)$. We consider the long-wavelength, low-energy limit of the problem, and obtain analytical results for low-energy $\mathcal{S}(\mathbf{k},\omega)$ and $N(\omega)$ and low-temperature $C_M(T)$. We recall here that all wave vectors are in units of inverse lattice spacing $1/a$, and all energies are in units of $\Omega_0=4SJ$.

We consider the low-energy form of the Green's functions first. At low energies $\omega,\omega_{\mathbf{k}}\ll 1$, self-energies (37)–(39) are given by

$$\Sigma^{11}_{\mathbf{k}}(\omega)=x\omega_{\mathbf{k}}[\rho(\omega)+2-\pi/2]-x\omega+O(\omega_{\mathbf{k}}\omega^2\rho^3),$$
$$\Sigma^{12}_{\mathbf{k}}(\omega)=x\omega_{\mathbf{k}}\gamma_{\mathbf{k}}[\rho(\omega)+\pi/2]+O(\omega_{\mathbf{k}}\omega^2\rho^3), \tag{48}$$

with

$$\rho(\omega)\simeq(2/\pi)\ln|\omega/4|-i,$$

which includes contributions from *s*- and *p*-wave scattering; the *d*-wave part is of higher order, $\Sigma_d\simeq O(\omega_{\mathbf{k}}^3)$ and $\omega_{\mathbf{k}}\simeq k/\sqrt{2}$. The importance of the projection of the unphysical states can be demonstrated one more time by a comparison of the above expressions with the "unprojected" ($H_z=0$) form of the self-energy,

$$\Sigma^{11}_{\mathbf{k}}(\omega)=x\omega_{\mathbf{k}}[\rho(\omega)-\pi/2]+x\omega_{\mathbf{k}}^2/\omega+O(\omega_{\mathbf{k}}\omega^2\rho^3), \tag{49}$$

which possesses an $\omega=0$ singularity. Notably the "physical" part of the expression containing the logarithm is not related to the unphysical states, and remains intact under the projection. As noted before, "on shell," $\omega=\omega_{\mathbf{k}}$, self-energies (48) and (49) coincide.[37] The off-diagonal $\Sigma^{12}_{\mathbf{k}}(\omega)$ is the same in both cases. It is also useful to note that the first-order Born approximation of the scattering problem would give very different results;

$$\Sigma^{11,Born}_{\mathbf{k}}(\omega)=-2x\omega_{\mathbf{k}},\quad \Sigma^{12,Born}_{\mathbf{k}}(\omega)=0, \tag{50}$$

with the imaginary part of the self-energy being $\sim O(xk\omega^2)$.

One can see that along with the "normal" softening and weak damping the full *T*-matrix consideration gives a nonlinear dispersion term and a damping $|\tilde{\gamma}_{\mathbf{k}}|/\omega_{\mathbf{k}}\simeq x$ which is only parametrically small with respect to the bare spectrum. A perturbative "on-shell" pole equation gives

$$\tilde{\omega}_{\mathbf{k}}+i\tilde{\gamma}_{\mathbf{k}}=\omega_{\mathbf{k}}+\Sigma^{11}_{\mathbf{k}}(\omega_{\mathbf{k}}),$$
$$\tilde{\omega}_{\mathbf{k}}=\omega_{\mathbf{k}}\left(1-x(\pi/2-1)+\frac{2x}{\pi}\ln\left|\omega_{\mathbf{k}}/4\right|\right), \tag{51}$$
$$\tilde{\gamma}_{\mathbf{k}}=-x\omega_{\mathbf{k}},$$

which already show that the spin-wave velocity in the effective medium is not well defined since the brackets in Eqs. (51) depend on $\mathbf{k}$. Moreover, the renormalization of the real part of the spectrum is dominated by the $\ln|\omega|$ term at low frequencies, and the brackets vanish at some wave vector

$$k_c^{-1}\sim\exp(\pi/2x). \tag{52}$$

Because of this one can naively suggest a vanishing of the spectrum[37] and an instability of the ground state toward some new phase. Such an instability is, of course, just a signature of the breakdown of the perturbation theory. One has to sum up all the "dangerous" terms using the Belyaev-Dyson equation [Fig. 1(b)] and Eq. (40), and analyze spectral functions(41).

The low-energy, long-wavelength forms of the Green's function [Eq. (40)], with self-energies from Eq. (48), are

$$G^{11}_{\mathbf{k}}(\omega)=G^{22}_{\mathbf{k}}(-\omega)\simeq\frac{\tilde{\omega}+\omega_{\mathbf{k}}(1+x[\rho(\omega)+2-\pi/2])}{\tilde{\omega}^2-\omega_{\mathbf{k}}^2(1+x[2\rho(\omega)+4-\pi])}, \tag{53}$$

$$G^{12}_{\mathbf{k}}(\omega)\simeq-\frac{x\gamma_{\mathbf{k}}\omega_{\mathbf{k}}[\rho(\omega)+\pi/2]}{\tilde{\omega}^2-\omega_{\mathbf{k}}^2(1+x[2\rho(\omega)+4-\pi])},$$

where $\tilde{\omega}=\omega(1+x)$, and $\rho(\omega)$ is defined in Eq. (48).

The diagonal spectral function in the same limit can be then written as

$$A^{11}_{\mathbf{k}}(\omega)\simeq\frac{1}{\pi}\frac{x\omega_{\mathbf{k}}(\tilde{\omega}+\omega_{\mathbf{k}})^2}{[\tilde{\omega}^2-\omega_{\mathbf{k}}^2a(\omega)]^2+(2x\omega_{\mathbf{k}}^2)^2}, \tag{54}$$

where we make use of imaginary part of the self-energies being $\mathrm{Im}\Sigma^{ij}_{\mathbf{k}}(\omega)\simeq-x\omega_{\mathbf{k}}$, and introduce a "stretching factor"

$$a(\omega)=1+x\left(\frac{4}{\pi}\ln\left|\omega/4\right|+4-\pi\right). \tag{55}$$

The energy at which this factor vanishes defines the disorder-induced energy scale

$$\omega_0\sim\exp\left(-\frac{\pi}{4x}\right), \tag{56}$$

below which the spectrum is overdamped.

A more detailed analysis of Eq. (54) gives the following picture. At wave vectors much larger than ω_0 ($\omega_{\mathbf{k}}\gg\omega_0$), that is, at wavelengths shorter than a characteristic length $l\sim e^{\pi/4x}$, the spectral function has three distinct regions in ω. First is a vicinity of a quasiparticle peak, $\omega\approx\tilde{\omega}_{\mathbf{k}}$,

$$A^{11}_{\mathbf{k}}(\omega)\approx\frac{2\omega_{\mathbf{k}}}{\pi}\frac{2x\omega_{\mathbf{k}}^2}{(\omega^2-\tilde{\omega}_{\mathbf{k}}^2)^2+(2x\omega_{\mathbf{k}}^2)^2}, \tag{57}$$

where the spectrum has a regular Lorentzian form with a pole at $\tilde{\omega}_{\mathbf{k}}$ and a width $\tilde{\gamma}_{\mathbf{k}}$ given by the perturbative result [Eq. (51)]. Second, in an intermediate range of energies $\omega_0<\omega\ll\tilde{\omega}_{\mathbf{k}}$, where the "stretching factor" is not too close to zero,

$$A^{11}_{\mathbf{k}}(\omega)\approx\frac{1}{\pi}\frac{x}{\omega_{\mathbf{k}}}\frac{1}{a(\omega)^2+4x^2}\approx\frac{1}{\pi}\frac{x}{\omega_{\mathbf{k}}}\text{const}, \tag{58}$$

one can approximate $a(\omega)$ by a constant since its dependence on ω is weak in this range. One can see that the spectral function in this region is independent of ω, and corresponds to an almost flat, shallow ($\sim x$) background of states. Third, in the vicinity of a ''localization peak'' $\omega\approx\omega_0$,

$$A^{11}_{\mathbf{k}}(\omega)\approx\frac{1}{4\pi}\frac{1}{x\omega_{\mathbf{k}}}\quad\text{at}\quad\omega=\omega_0, \tag{59}$$

$$A^{11}_{\mathbf{k}}(\omega)\approx\frac{\pi}{16}\frac{1}{\omega_{\mathbf{k}}}\frac{1}{x\ln^2|\omega|}\quad\text{at}\quad\omega\ll\omega_0,$$

the spectral function rises sharply from the shallow background states $\sim x$ [Eq. (58)] to a peak of the height $\sim 1/x$, and then vanishes in a singular fashion as ω approaches zero. Note that this peak is non-Lorentzian, and its position ($\omega=\omega_0$) is independent of the value of $\mathbf{k}$.

Thus, besides the lack of the Lorentz invariance of the quasiparticle part of the spectrum of Eq. (51), every $\mathbf{k}$ mode redistributes some of its weight from the energy $\sim\omega_{\mathbf{k}}$ to a flat background of states between $\tilde{\omega}_{\mathbf{k}}$ and ω_0 and to a peak at $\omega=\omega_0$. Such a behavior is similar to other problems of linearly dispersive excitations in the presence of disorder in two dimensions, and should be interpreted as the signature of localization.[44,54] Then the characteristic length

$$l\sim\exp\left(\frac{\pi}{4x}\right) \tag{60}$$

is to be understood as a localization length of the spin waves in our problem.

The truly intriguing question is what happens at wavelengths of order of l and beyond. In our approach for $k\lesssim l^{-1}$, the quasiparticle and localization peaks merge into a broad incoherent peak that disperses in momentum space. One can see that at $k\sim\omega_0<l^{-1}$, factor $a(\omega)$ is negative and the ''pole'' in Eq. (54) becomes purely imaginary. However, since $a(\omega)$ is ω dependent this peak is non-Lorentzian, and thus cannot be associated with a ''simple'' diffusive mode. Thus we observe an overdamped, non-Lorentzian diffuse like excitation with a characteristic width of the order of $\omega_{\mathbf{k}}$ and a peak position roughly at $\omega\lesssim\omega_{\mathbf{k}}$. We have to remark here that the nature of states at the wavelength above the localization length might be beyond the ability of our approach, and a proper description of them may require a different, nonperturbative type of study.

Thus the structure of the spectral function we discuss above demonstrates an unusual, nonhydrodynamic type of behavior of the spin-excitation spectrum of a diluted 2D AF. The strong influence of disorder in the low-energy excitations in two dimensions results in the failure of the averaging procedure, which effectively restores translational invariance, to recover the long-wavelength excitation spectrum of this effective medium. Already at energies much larger than the disorder-induced scale $\omega\sim k\gg\omega_0$, one finds a departure from hydrodynamics: while ''quasiparticle'' excitation can be found, it does not disperse linearly with $\mathbf{k}$, and its damping is neither hydrodynamic nor quasiparticlelike. More importantly, *above* a characteristic wavelength l no hydrodynamic description of excitations is possible. Low-frequency modes do exist in some form, but they cannot be classified in terms of an effective wave vector; thus the long-wavelength propagation is entirely diffusive.

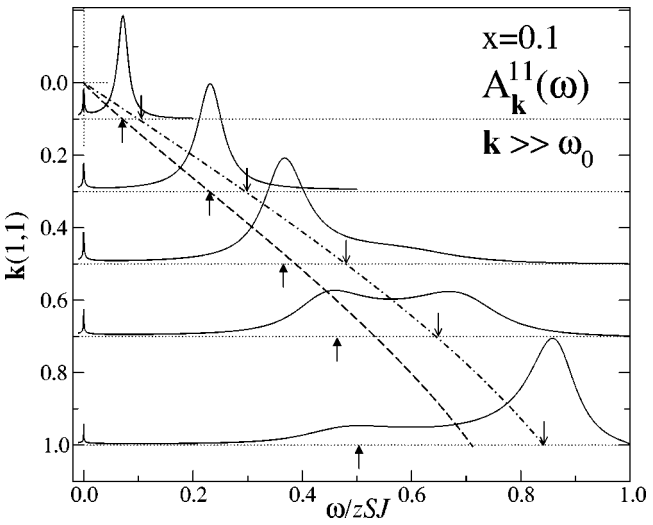

FIG. 2. The spectral function $A^{11}_{\mathbf{k}}(\omega)$ for the wave vectors $\mathbf{k}=0.1$, 0.3, 0.5, 0.7, and 1.0, all $\gg\omega_0$ along the (1,1) direction $\mathbf{k}$ is in units of $1/a$. The dash-dotted line is the bare spin-wave energy, and the arrows pointing down are the positions of the original δ-function peaks. The dashed line is the renormalized spin-wave dispersion [Eq. (51)], and the arrows pointing up show the actual positions of the peaks for selected wave vectors. $A^{11}_{\mathbf{k}}(\omega)$ for each $\mathbf{k}$ is normalized to fit the picture.

In addition, the spectra at $k\gg\omega_0$ are not exhausted by the quasiparticle peak. They also consist of a background of localized states and the localization peak described in Eqs. (58) and (59).

The spectral function $A^{11}_{\mathbf{k}}(\omega)$ obtained from ''full'' expressions for the Green's function [Eq. (40)] and self-energies (35)–(39) without taking the low-energy limit is shown in Figs. 2–4 for a number of wave vectors along the (1,1) direction of the Brillouin zone for a representative value of the impurity concentration $x=0.1$. The purpose of these pictures is to demonstrate the features we discussed using the long-wavelength form of $A^{11}_{\mathbf{k}}(\omega)$. The amplitude of each $A_{\mathbf{k}}(\omega)$ curve is normalized to fit the picture, and therefore the relative heights of the curves bear no meaning. These figures also show the bare spin-wave energy (dashed-dotted line), with arrows pointing down showing the positions of ''unperturbed'' δ-function peaks. The dashed line corresponds to a perturbative renormalized spin-wave dispersion [Eq. (51)], while arrows pointing up show the actual positions of the peaks for selected wave vectors. The figures show the spectral function within the different ranges of $\mathbf{k}$ relative to ω_0, $\mathbf{k}\gg\omega_0$, $\mathbf{k}\gtrsim\omega_0$, and $\mathbf{k}\lesssim\omega_0$, respectively. The latter can be calculated using Eq. (56), which gives $\omega_0(x=0.1)\sim 10^{-3}$.

Figure 2 shows the spectral function $A^{11}_{\mathbf{k}}(\omega)$ for wave

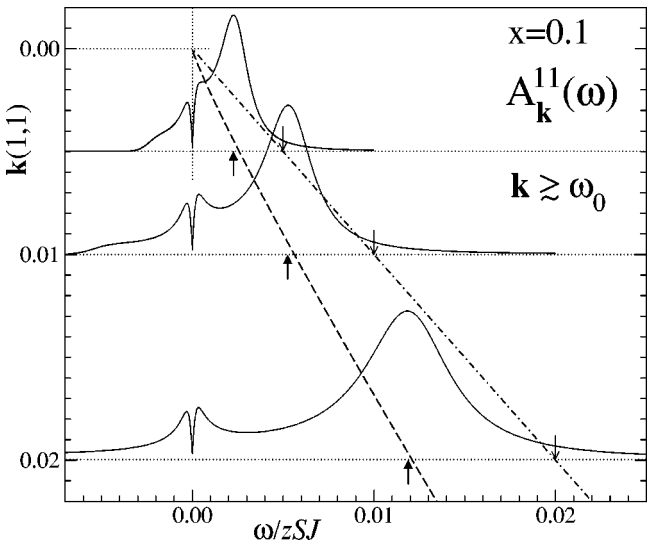

FIG. 3. The spectral function $A_{\mathbf{k}}^{11}(\omega)$ for wave vectors $\mathbf{k}=0.005$, 0.01, and 0.02 along the (1,1) direction; $\mathbf{k}=0.005$ is of the order of ω_0. The dash-dotted line, the dashed line, and the arrows are as in Fig. 2. $A_{\mathbf{k}}^{11}(\omega)$ for each $\mathbf{k}$ is normalized to fit the picture.

vectors $\mathbf{k}=0.1$, 0.3, 0.5, 0.7, and 1.0 along the (1,1) direction [$\mathbf{k}$ is in units of $1/a$, so that the corner of the Brillouin zone is (π,π)]. One can see that the quasiparticle peak follows the renormalized spin-wave dispersion [Eq. (51)] at low $\mathbf{k}$ very closely. At higher values of $\mathbf{k}$ a higher-energy subband develops, and the spectrum evolves into the ''camel''-like structure discussed extensively in Ref. 15. The origin of this high-energy structure is in the presence of a high-energy resonance state ($\omega_{res} \simeq J$) around an impurity,[46] which is unrelated to the low-energy physics of the system. Since our low-energy consideration does not take this high-energy feature into account, the position of the lower peak in this structure deviates from the long-wavelength dispersion [Eq. (51)]

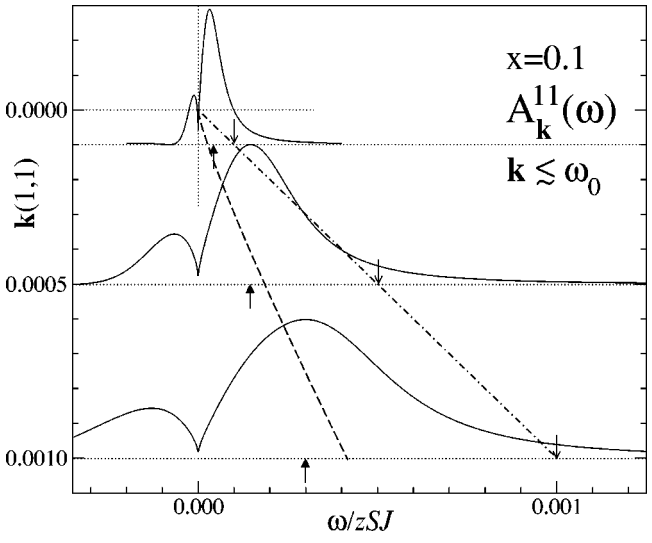

FIG. 4. The spectral function $A_{\mathbf{k}}^{11}(\omega)$ for wave vectors $\mathbf{k}=0.0001$, 0.0005, and 0.001, all $<\omega_0$, along the (1,1) direction. The dash-dotted line, the dashed line, and the arrows are as in Fig. 2. $A_{\mathbf{k}}^{11}(\omega)$ for each $\mathbf{k}$ is normalized to fit the picture.

at larger $\mathbf{k}$. The low-energy localization peak and the background are already noticeable in Fig. 2 despite the high-energy scale.

Figure 3 shows the spectral function $A_{\mathbf{k}}^{11}(\omega)$ for wave vectors $\mathbf{k}=0.005$, 0.01, and 0.02, with the smallest wave vector being of the order of ω_0. One can clearly see the features we discussed in Eqs. (57)–(59): the broadened quasiparticle peak, the localization peak, and the states between them. The quasiparticle peak continue to follow a renormalized spin-wave dispersion [Eq. (51)]. As $\mathbf{k}$ decreases, all the mentioned structures merge.

Figure 4 shows the spectral function $A_{\mathbf{k}}^{11}(\omega)$ for wave vectors $\mathbf{k}=0.0001$, 0.0005, and 0.001; all are smaller than ω_0. As we discussed above, the quasiparticle and localization peaks merge, and give a broad, overdamped, non-Lorentzian diffusive peak. In other words, one may not represent the Green's function in this region as a sum of coherent and incoherent contributions $G_{\mathbf{k}}^{coh}(\omega)+G_{\mathbf{k}}^{incoh}(\omega)$; it seems that only the second part survives. The peak position deviates from the perturbative renormalized spin-wave dispersion [Eq. (51)], and thus indicates the region where the perturbation theory breaks down.

The off-diagonal spectral function $A_{\mathbf{k}}^{12}(\omega)$ should possess features similar to the one of the diagonal spectral function. The low-energy, long-wavelength form of $A_{\mathbf{k}}^{12}(\omega)$ is given by

$$A_{\mathbf{k}}^{12}(\omega) \simeq \frac{1}{\pi} \frac{x\gamma_{\mathbf{k}}\omega_{\mathbf{k}}[\omega_{\mathbf{k}}^2 b(x)-\tilde{\omega}^2]}{[\tilde{\omega}^2-\omega_{\mathbf{k}}^2 a(\omega)]^2+(2x\omega_{\mathbf{k}}^2)^2}, \tag{61}$$

where $b(x)=[1-2x(\pi-2)]$. Note that $A_{\mathbf{k}}^{12}(\omega)$ is not a positively defined function; it changes sign as a function of ω at $\omega=\omega_{\mathbf{k}}\sqrt{b(x)}/(1+x)$. Another important difference from $A_{\mathbf{k}}^{11}(\omega)$ is that $A_{\mathbf{k}}^{12}(\omega)$ is odd under the transformation $\mathbf{k}\rightarrow\mathbf{k}+\mathbf{Q}$, and thus has opposite sign in the first and second magnetic Brillouin zones.

A detailed analysis of $A_{\mathbf{k}}^{12}(\omega)$ in different regions of $\omega_{\mathbf{k}}$ and ω shows that in the vicinity of a quasiparticle peak $A_{\mathbf{k}}^{12}(\omega)$ has an additional smallness of order x in comparison with $A_{\mathbf{k}}^{11}(\omega)$, but it is of the same order in the ''intermediate'' ($\omega<\omega_{\mathbf{k}}$) and low-energy regions, where it can be approximated as

$$A_{\mathbf{k}}^{12}(\omega) \approx \frac{1}{\pi} \frac{x\gamma_{\mathbf{k}}}{\omega_{\mathbf{k}}} \frac{1}{a(\omega)^2+4x^2}, \tag{62}$$

with the behavior above, at, and below the localization peak identical to the one of $A_{\mathbf{k}}^{11}(\omega)$ [Eqs. (58) and (59)].

Figure 5 gives an example of the structure of the off-diagonal spectral function $A_{\mathbf{k}}^{12}(\omega)$, obtained from Eqs. (40) and (35)–(39) without taking the low-energy limit for wave vectors $\mathbf{k}=0.1$, 0.3, 0.5, 0.7, and 1.0. Features discussed in the preceding paragraphs—such as changes of the sign, the low-energy localization peak, and background states—are clearly seen in this spectral function.

The transverse component of the neutron-scattering dynamical structure factor $\mathcal{S}^{+-}(\mathbf{k},\omega)$ is directly related to the

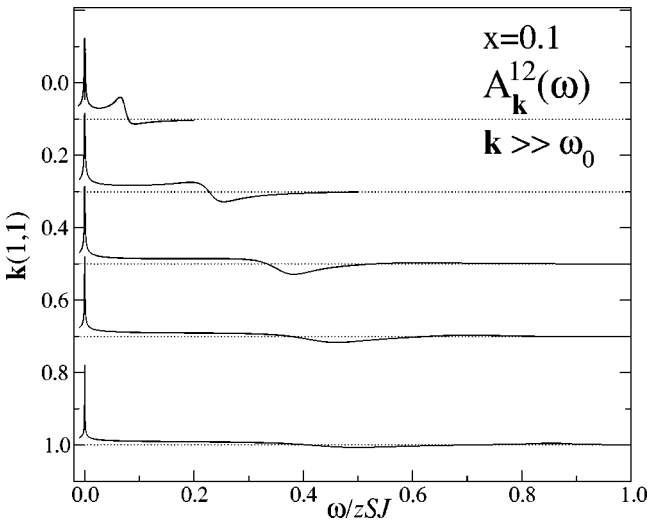

FIG. 5. The spectral function $A^{12}_{\mathbf{k}}(\omega)$ for wave vectors $\mathbf{k}=0.1, 0.3, 0.5, 0.7$, and 1.0, all $\gg\omega_0$ along the (1,1) direction. $A^{12}_{\mathbf{k}}(\omega)$ for each $\mathbf{k}$ is normalized to fit the picture.

linear combination of the magnon spectral functions $A^{11}_{\mathbf{k}}(\omega)$, $A^{22}_{\mathbf{k}}(\omega)[=A^{11}_{\mathbf{k}}(-\omega)]$, and $A^{12}_{\mathbf{k}}(\omega)$, as given by Eq. (43). It therefore must contain all the features of the spectral functions we discuss here. Figure 6 shows an example of our result for $\mathcal{S}^{+-}(\mathbf{k},\omega)$ vs ω at $\mathbf{k}=0.1$, that is, in the ''nuclear'' Brillouin zone, for $x=0.05$. The long dashed arrow shows the initial position of the δ-functional peak. Since $\pm\omega_0$ are very small in this case, the localization peak is seen as a single spike at $\omega=0$, but the flat background of states is clearly visible below the quasiparticle peak.

However, the actual observation of anomalous features of the spectra can be complicated for two reasons. First, the structure factor contains a kinematic form factor which enhances the spectral function combination by $\simeq 2/\omega_{\mathbf{k}}$ close to $\mathbf{k}=\mathbf{Q}$, and suppresses it by $\simeq\omega_{\mathbf{k}}/2$ close to $\mathbf{k}=0$. Second, as

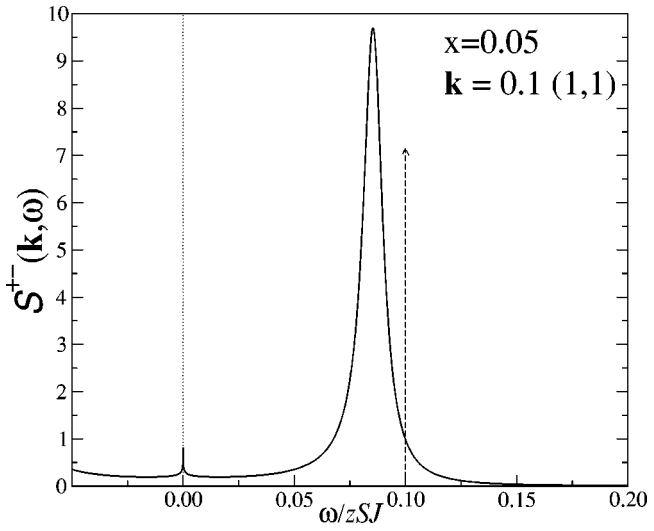

FIG. 6. Transverse component of the neutron-scattering dynamical structure factor $\mathcal{S}^{+-}(\mathbf{k},\omega)$, $\mathbf{k}=0.1$, and $x=0.05$. The long-dashed arrow shows the initial position of the δ-functional peak.

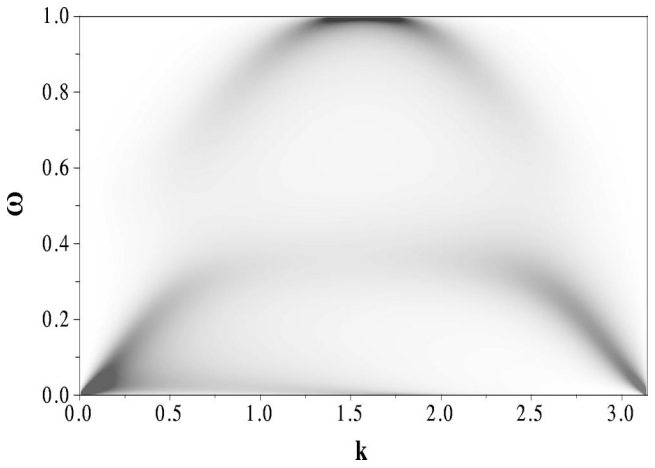

FIG. 7. The intensity map of $\pi SA^{\Sigma}_{\mathbf{k}}(\omega)$, in the $\mathbf{k}$-ω plane for $\mathbf{k}$ from (0,0) to (π,π) in the (1,1) direction, and from $\omega=0$ to $\omega=1$ for $x=0.25$.

we show below, the sum of the spectral functions entering $\mathcal{S}^{+-}(\mathbf{k},\omega)$ is ''less anomalous'' close to $\mathbf{k}=\mathbf{Q}$ than at $\mathbf{k}\to 0$. That is, the quasiparticle part of the spectrum is abnormally broadened and disperses nonlinearly for both $\mathbf{k}\to 0$ and $\mathbf{k}\to\mathbf{Q}$, while the low-energy localization features are suppressed in the vicinity of $\mathbf{Q}$ due to cancellation between the diagonal and off-diagonal contributions.

One can show explicitly using the low-energy, long-wavelength limit of the sum of spectral functions $[A^{11}_{\mathbf{k}}(\omega)+A^{22}_{\mathbf{k}}(\omega)+2A^{12}_{\mathbf{k}}(\omega)]$ given by

$$A^{\Sigma}_{\mathbf{k}}(\omega)\equiv\sum_{\alpha\beta=1,2}A^{\alpha\beta}_{\mathbf{k}}(\omega)\simeq\frac{2x\omega_{\mathbf{k}}}{\pi}\times\frac{\tilde{\omega}^2(1-\gamma_{\mathbf{k}})+\omega^2_{\mathbf{k}}(1+\gamma_{\mathbf{k}})-2x\gamma_{\mathbf{k}}\omega^2_{\mathbf{k}}(\pi-2)}{[\tilde{\omega}^2-\omega^2_{\mathbf{k}}a(\omega)]^2+(2x\omega^2_{\mathbf{k}})^2},\tag{63}$$

that, aside from the kinematic form factor, the dynamical structure factor should be different in the first ($\mathbf{k}\to 0$) magnetic Brillouin zone,

$$A^{\Sigma}_{\mathbf{k}}(\omega)\approx\frac{1}{\pi}\frac{4x\omega^3_{\mathbf{k}}}{[\tilde{\omega}^2-\omega^2_{\mathbf{k}}a(\omega)]^2+(2x\omega^2_{\mathbf{k}})^2},\tag{64}$$

and the second ($\mathbf{k}\to\mathbf{Q}$) magnetic Brillouin zone

$$A^{\Sigma}_{\mathbf{k}}(\omega)\approx\frac{1}{\pi}\frac{4x\omega_{\mathbf{k}}\tilde{\omega}^2}{[\tilde{\omega}^2-\omega^2_{\mathbf{k}}a(\omega)]^2+(2x\omega^2_{\mathbf{k}})^2},\tag{65}$$

due to the asymmetry of $A^{12}_{\mathbf{k}}(\omega)$ to $\mathbf{k}\to\mathbf{k}+\mathbf{Q}$. One can see that around the quasiparticle peak $\omega\simeq\omega_{\mathbf{k}}$ these expressions are identical, and are simply equal to the diagonal spectral function [Eq. (57)]; however but at lower energies for $\mathbf{k}\sim\mathbf{Q}$, the localization features are suppressed by the factor of ω^2.

This asymmetry is demonstrated in Fig. 7, which shows the intensity map of $\mathcal{S}^{+-}(\mathbf{k},\omega)\cdot\omega_{\mathbf{k}}/(1-\gamma_{\mathbf{k}})=\pi SA^{\Sigma}_{\mathbf{k}}(\omega)$,

that is, the structure factor divided by the kinematic form factor, in the $\mathbf{k}-\omega$ plane across the Brillouin zone in the (1,1) direction from $\mathbf{k}=0$ to $\mathbf{k}=(\pi,\pi)$, for $x=0.25$. The higher intensity corresponds to the higher value of the function. One can clearly see all the features of the spectrum described in this section: the resonance and its splitting from the dispersive mode at high energies, the low-energy damped spin-wave mode in both the center and the corner of the Brillouin zone, and the asymmetric background of localized states with the low-energy peak at the bottom. The nonlinearity of the quasiparticle mode also seems to be quite visible, though the actual detection of it or of the abnormal *k*-dependence of the damping can be a challenging experimental problem.

The density of states of spin excitations can be easily calculated using Eqs. (44) and (40). We recall that for a pure 2D system with a linear spectrum of excitations, the low-energy density of states is a linear function of ω and, in our case,

$$N(\omega)=\frac{2}{\pi}\omega. \tag{66}$$

Evidently, low-energy localized states should strongly affect $N(\omega)$, and one readily finds anomalous corrections at the level of a perturbative analysis of the Green's function. If one uses the full *T*-matrix form of the self-energy but expands the Green's function in *x*,

$$G^{11}_{\mathbf{k}}(\omega)\simeq G^{0,11}_{\mathbf{k}}(\omega)+G^{0,11}_{\mathbf{k}}(\omega)\Sigma^{11}_{\mathbf{k}}(\omega)G^{0,11}_{\mathbf{k}}(\omega), \tag{67}$$

one immediately obtains a constant correction

$$N(\omega)=\frac{2}{\pi}\omega+xC+O(x\omega\ln|\omega|), \tag{68}$$

which also implies a finite density of states at $\omega=0$. A more sensible result can be obtained without using an *x* expansion from the long-wavelength expression for the spectral function $A^{11}_{\mathbf{k}}(\omega)$ [Eq. (54)],

$$N(\omega)=\frac{2}{\pi}\omega+xC_1/[a(\omega)^2+4x^2]+O(x\,\omega\ln|\omega|), \tag{69}$$

where $a(\omega)$ is the same "stretching factor" [Eq. (55)] we used in Eqs. (54), (58), and (61)–(65). At $\omega\gg\omega_0$, $a(\omega)\approx$const, and we are back to the previous result given by *x*-expansion perturbation theory [Eq. (68)]. At $\omega\approx\omega_0$ the density of states has a peak of height $\sim 1/x$ whose origin is evident: low-energy nondispersive localized states contribute to it altogether. At $\omega\ll\omega_0$ the density of states vanishes as $N\propto 1/(x\ln|\omega|)^2$. Such a strong dependence of the result on the degree of approximation is reminiscent of the dispute over $N(\omega)$ for certain types of disorder in 2D systems with linear excitation spectra,[44,52] where different approaches result in drastically different answers for the low-energy part of the density of states.

Figure 8 shows results for the density of states for $x=0$ (pure system, dashed curve), $x=0.1$, and $x=0.2$. The dotted curves show $N(\omega)$ given by Eq. (69) with $C_1=4/\pi^{3/2}$, which is obtained from a long-wavelength expression for spectral

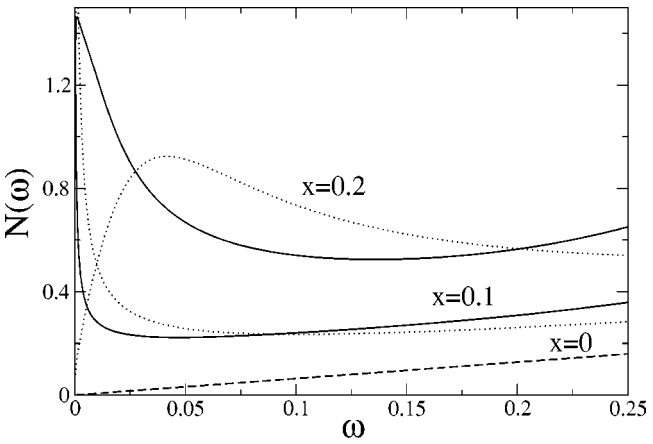

FIG. 8. Density of states $N(\omega)$ vs ω for $x=0$ (pure system, dashed curve), $x=0.1$, and $x=0.2$ (dotted and solid curves). Dotted curves show the long-wavelength result [Eq. (69)] with $C_1=4/\pi^{3/2}$. The solid curves show the result of numerical integration using the full Green's function [Eq. (40)].

function (54). The solid curves are the result of a numerical integration using the "full" Green's function [Eq. (40)]. While the overall agreement of these curves is very good, there is a significant discrepancy at low energies which has the following origin. In the long-wavelength limit we regarded the localization peak at $\omega=\omega_0$ as nondispersive, whereas, at larger $\mathbf{k}$, close to the magnetic Brillouin-zone boundary, it disperses down to $\omega\sim\omega_0^2\sim e^{-\pi/2x}\ll\omega_0$. This can also be noted in Fig. 7. As a result of such a dispersion, the peak in the density of states at ω_0 is spread to lower energies. Technically, there is a term in the denominator of the Green's function $\sim x^2\rho(\omega)^2\omega_{\mathbf{k}}^4$, negligible at low $\mathbf{k}$, which leads to such a behavior. Since this term is of the order of x^2 and our approach does not take all such terms into account, we have no certainty of whether this is a spurious feature or not. As we show below, this discrepancy does not affect any of our conclusions.

In this context it is interesting to note that the constant term in the density of states, which is a prominent feature of all three "full," long-wavelength, and perturbative results, is directly related to the flat background of states below the quasiparticle peak in the spectral function. The localization-peak feature of the spectral function is responsible for the peak in $N(\omega)$ at low ω.

The calculation of the magnetic contribution to the specific heat, using results for $N(\omega)$ and Eq. (45), is straightforward. For the pure system, $C_M(T)\sim T^2$, because of two dimensionality. The anomalous density of states results in a quasilinear correction to this. Using the long-wavelength expression for the density of states, for such a correction we obtain

$$\delta C_M(T)\approx\frac{A(x)}{x}\,\frac{T}{\ln^2|T/\omega_0|+\pi^2/4}, \tag{70}$$

where $A(x)$ is a weak function of *x*. At $T\gg\omega_0$ (T is also in units of Ω_0) this gives

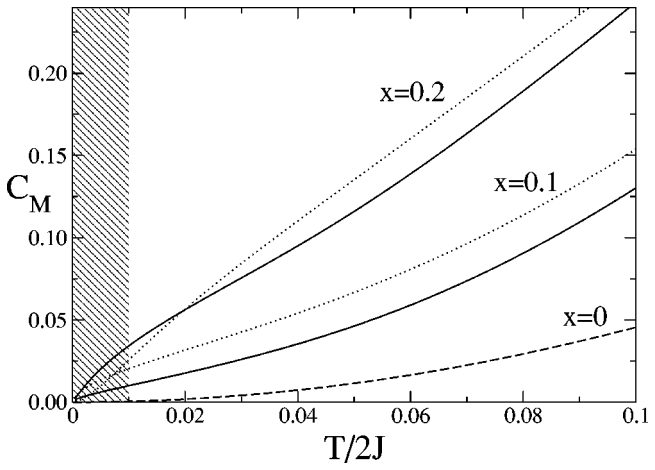

FIG. 9. $C_M(T)$ vs T for a spin-1/2 system for $x=0$ (dashed curve), $x=0.1$, and $x=0.2$ (dotted and solid curves). Dotted curves show the long-wavelength results, and solid curves the result of numerical integration using the full Green's function [Eq. (40)]. The dashed sector shows the 3D crossover temperature region $T \lesssim \sqrt{JJ_\perp}$ for $J_\perp = 10^{-4}J$.

$$\delta C_M(T) \approx xT \times \text{const.} \tag{71}$$

Figure 9 shows our results for the magnetic specific heat of a spin-1/2 system ($\Omega_0 = 2J$) vs T for $x=0$ (dashed curve), $x=0.1$, and $x=0.2$. Dotted curves are results from the long-wavelength expression for $N(\omega)$, and solid curves are from numerical integration using Eqs. (40) and (45). One can see that the results are very close, and point to the same behavior. The dashed sector shows the temperature region $T \lesssim \sqrt{JJ_\perp}$ where the crossover to 3D behavior (which provides higher powers of T to C_M) should occur. We use the value $J_\perp = 10^{-4}J$, characteristic for the cuprates.

Realistically, this picture should overlap with the phonon contribution to the specific heat. One would expect phonons to remain essentially three dimensional even in layered materials with characteristic T^3 contributions to the specific heat at low temperatures, and thus be negligible in comparison with T^2 and xT terms. However, in the case of cuprates the phonon Debye energy is of the order of 400 K,[55] which is significantly lower than $2J \simeq 3000$ K. This causes the phonon part of $C(T)$ deviate from the T^3 behavior at about 20 K, that is around the 3D crossover temperature for a magnetic subsystem. Because of the much lower Debye energy, the specific heat in cuprates is dominated by the phonon part.[55] Therefore, in order to observe the anomalous quasilinear contribution of the localized states to $C(T)$, one needs to use the "reference" material $x=0$, and subtract $C_{x=0}(T)$ from the results for the systems with $x>0$ (we assume that impurities do not introduce dramatic changes in the low-energy phonon spectra). Another route is to find a quasi-2D system with a much lower value of J (of the order or less than Debye energy for phonons) which would allow a direct observation of the xT anomaly from localized states.

The finite value of the interplane coupling, together with the small anisotropy gaps, leads to a finite value of the ordering temperature T_N whose dependence on the impurity concentration is considered in Sec. IV. The effect of the 3D coupling in the dynamic properties, briefly mentioned above in the context of the specific heat, is as follows. The energy scale introduced by the interplane coupling $\tau = J_\perp/2J$ is $\omega_{3D} = \sqrt{4\tau}$, as seen from Eqs. (5) and (13); therefore it is rather small for the realistic systems of interest (for LCO, $\omega_{3D} \simeq 0.01$ in the units of the magnon bandwidth). We show in Appendix B that the 3D corrections to the 2D scattering are given by $O(\tau \ln \tau)$, which is truly negligible ($\sim 10^{-4}$ for LCO). Therefore, the only appreciable correction to the dynamic properties from 3D coupling is the low-energy cutoff of the logarithmic terms in the self-energy at $\omega = \omega_{3D}$. As we describe in Appendix E

$$\rho_{3D}(\omega) \simeq \frac{1}{\pi} \ln \left| \frac{\tau}{16} \right| - i \frac{\omega}{\pi \sqrt{\tau}} \quad \text{at} \quad \omega \ll \omega_{3D}; \tag{72}$$

that is, below the 3D energy scale the real part is a constant and the imaginary part has an extra power of ω in comparison with the pure 2D form of $\rho(\omega)$. $\rho(\omega)$ remains essentially two dimensional at $\omega > \omega_{3D}$. Evidently, this proves that the 3D coupling has little or no effect on the properties of the spectral functions, dynamical structure factor, or density of states at $\omega > \omega_{3D}$.

However, the 3D coupling does affect some of the localization features in the following way. Below the 3D energy scale the "stretching factor" [Eq. (55)] saturates at the value $a(\omega_{3D})$, and the imaginary part of the self-energy acquires an extra power of ω. In other words, it should be understood as a competition between disorder-induced and 3D energy scales. Therefore, there are two regions of x. First, when x is small enough, $0 < x \lesssim x^* \sim 1/\ln \tau^{-1}$, so that $a(\omega_{3D}) > 0$. In this region the well-defined spin waves can be found deep in the low-$\mathbf{k}$, low-ω region ($k, \omega \ll \omega_{3D}$), similar to the quasi-1D problem.[47] Concentration x^* is defined from the equality of the energy scales $e^{-\pi/4x} = \sqrt{\tau}$ which gives $x^* \sim 1/\ln \tau^{-1}$. The localization peak in the spectral function at $\omega \sim \omega_0 \sim J e^{-\pi/4x}$ in the low-ω, $\mathbf{k} \gg \omega$ region, will be replaced by

$$A_{\mathbf{k}}^{3D,11}(\omega) \approx \frac{1}{\pi} \frac{x\omega}{\omega_{\mathbf{k}}} \frac{1}{a(\omega_{3D})^2} \quad \text{at} \quad \omega \ll \omega_{3D}, \tag{73}$$

which smoothly vanishes as ω goes to zero instead of showing a peak. However, the nonlinearity of the spectrum, the abnormal damping of the quasiparticles, and the flat background of the localized states below $\tilde{\omega}_{\mathbf{k}}$ are all in the 2D region of $\mathbf{k} - \omega$ space ($\omega > \omega_{3D}$), and will remain intact.

The second region is $x \gtrsim x^*$ where $a(\omega_{3D}) < 0$. In this region the pole at low $\mathbf{k}$ and low ω becomes pure imaginary as in the 2D case, and the localization peak for low-ω, $\mathbf{k} \gg \omega$ reappear above the 3D scale. Above the concentration x^* all the low-energy excitations are incoherent, because the 2D disorder-induced energy scale ω_0 (localization length l) is larger (shorter) than the 3D energy scale ω_{3D} (length scale $1/\sqrt{\tau}$) so the spin waves lose their coherence before they can propagate in three dimensions. A self-consistent calculation

is required to determine accurately the value of x^* and the details of the 3D to 2D crossover. Our estimation gives $x^* \sim 0.1$–0.2 for $\tau \sim 10^{-4}$.

Thus we find that a 3D coupling for the realistic materials will modify the 2D density of states, structure factor, and specific heat only at the energies (temperatures) $\omega < \omega_{3D} \simeq 0.01$, and at impurity concentrations $x < x^* \simeq 0.1-0.2$. The estimated value of the 3D coupling τ_c which would make x^* larger than the percolation threshold is $\tau_c \sim 0.01$.

The consideration given above also applies to the case of small anisotropies, introducing gaps in the spectrum with a modified $\tau = \tau_{eff}$ accumulating the total effect of the gaps and 3D coupling. It should be noted that the incoherence comes from the averaging procedure which converts the dissipation of momentum into the dissipation of the energy. Therefore, the overdamped excitations should be understood to be diffusive. It is interesting that it requires 2D ''strong'' disorder to restrict the number of Euclidean paths for spin waves and to break down the description of the problem in terms of an effective medium.

IV. STATIC PROPERTIES

Static properties such as the average staggered magnetization $M(x,T)$, the Néel temperature $T_N(x)$, and the 2D correlation length $\xi(T,x)$ are considered in this section. The average on-site magnetic moment [Eq. (46)] for randomly diluted AF's with averaging over magnetic sites $M(x) = \Sigma_i |S_i^z|/N_m$, (see Ref. 48), can be expressed through the integral of the spectral functions [Eq. (41)] as

$$M(x,T) = S - \Delta - \delta M(x,T), \tag{74}$$

$$\delta M(x,T) = \sum_{\mathbf{k}} \int_{-\infty}^{\infty} \frac{n_B(\omega) \mathrm{d}\omega}{\omega_{\mathbf{k}}} [A^{11}_{R,\mathbf{k}}(\omega) - \gamma_{\mathbf{k}} A^{12}_{R,\mathbf{k}}(\omega)],$$

where $\Delta = \Sigma_{\mathbf{k}} v_{\mathbf{k}}^2 \simeq 0.1966$ is the zero-point spin deviation, $n_B(\omega) = [e^{\omega/T} - 1]^{-1}$ is the Bose distribution function, and subscript R denotes ''retarded.'' Note that one should not expect this formula to be valid at a large doping level x close to x_p, since our approach neglects decoupled clusters and interactions of impurities. However, at not too large x these effects should be negligible, and one would expect Eq. (74) to be adequate. We would also like to note here that our definition of $M(x,T)$ is physically equivalent to the ''quantum-mechanical factor'' of the averaged staggered magnetization, the definition used in a recent Monte Carlo study.[26] In other words, the ''classical'' (''geometrical'') effect of dilution on magnetization, which simply accounts for the decrease of the magnetic substance, is multiplicative to the quantum effects, and is not taken into account in Eq. (74).

First we address the question of the presence of explicit divergences in integral equation (74), which would point to the instability of the long-range order discussed in Refs. 30 and 37. At $T=0$, $n_B(\omega) = -\theta(-\omega)$, and the impurity-induced quantum reduction of the magnetization, which can be interpreted as a result of the ''condensation of magnons,'' is given by

$$\delta M(x) = -\sum_{\mathbf{k}} \int_{-1}^{0} \frac{d\omega}{\omega_{\mathbf{k}}} [A^{11}_{R,\mathbf{k}}(\omega) - \gamma_{\mathbf{k}} A^{12}_{R,\mathbf{k}}(\omega)], \tag{75}$$

where the spectral functions are zero outside of the magnon band $\omega^2 > 1$. Since the perturbative result [Eq. (51)] suggests the instability at small wave vectors, long-wavelength expressions for the spectral functions can be used for our analysis. From the form of the spectral functions in Eqs. (54) and (61) one can readily see that the integral over ω is always finite. The integration over $\mathbf{k}$ is two dimensional, but has a factor of $1/\omega_{\mathbf{k}}$ in the integrand. From our expression of the spectral functions in the intermediate and localization peak energy ranges [Eqs. (58), (59), and (62)], one may suggest that there is another $1/\omega_{\mathbf{k}}$ in the integrand which would lead to the logarithmic divergency. However, these expression are obtained by neglecting ω^2 in comparison with $\omega_{\mathbf{k}}^2$, and thus are valid only at $\omega_{\mathbf{k}} \gg \omega$. At lower $\mathbf{k}$ the convergence of the integral is restored. To show this more explicitly, one can use the x-expanded form of the Green's function [Eq. (67)] for $A^{11}_{R,\mathbf{k}}(\omega)$, and an equivalent expression for $A^{12}_{R,\mathbf{k}}(\omega)$:

$$G^{12}_{\mathbf{k}}(\omega) \simeq G^{0,22}_{\mathbf{k}}(\omega) \Sigma^{12}_{\mathbf{k}}(\omega) G^{0,11}_{\mathbf{k}}(\omega). \tag{76}$$

Since all Σ's are linear in x, this provides an expression for the term linear in x in staggered magnetization:

$$\delta M(x) \simeq xB = -\sum_{\mathbf{k}} \int_{-1}^{0} \frac{\mathrm{d}\omega}{\pi \omega_{\mathbf{k}}} \left[\frac{\mathrm{Im}\, \Sigma^{11}_{R,\mathbf{k}}(\omega)}{(\omega - \omega_{\mathbf{k}})^2} + \frac{\gamma_{\mathbf{k}} \mathrm{Im}\, \Sigma^{12}_{R,\mathbf{k}}(\omega)}{\omega^2 - \omega_{\mathbf{k}}^2} \right] + \sum_{\mathbf{k}} \frac{\gamma_{\mathbf{k}} \mathrm{Re}\, \Sigma^{12}_{\mathbf{k}}(\omega_{\mathbf{k}})}{2\omega_{\mathbf{k}}^2}. \tag{77}$$

In the long-wavelength limit this gives

$$\delta M(x) \simeq xB \simeq \frac{x}{\pi} \sum_{\mathbf{k}} \int_0^1 \mathrm{d}\omega \left[\frac{1}{(\omega + \omega_{\mathbf{k}})^2} + \frac{1}{\omega^2 - \omega_{\mathbf{k}}^2} \right] + \frac{x}{\pi} \sum_{\mathbf{k}} \frac{1}{\omega_{\mathbf{k}}} \left[\ln \left| \frac{\omega_{\mathbf{k}}}{4} \right| - \pi^2/4 \right], \tag{78}$$

where the strongest divergency of the integrand is $\ln k dk$ and all integrals are convergent.

Numerical integration of the expression in Eq. (77), without the long-wavelength approximation, gives the suppression rate of the staggered magnetization $M(x) \simeq M(0) - Bx$ with $B = 0.209(8)$. For $S = 1/2$ this gives the slope of the normalized staggered magnetization $M(x)/M(0) \simeq 1 - Bx/(S-\Delta) \simeq 1 - 0.691(5)x$. It is interesting to note that the second Born approximation of the impurity scattering gives a three times smaller rate $B_{Born} = 0.0725$, showing the necessity for a full T-matrix treatment of the problem. The estimation of B, given in Ref. 37 using the $1/z$ approximation for an expression similar to our Eq. (77), provides even smaller $B_{1/z} \simeq 1/z^2 = 0.0625$ showing yet another inadequacy of that work.

We have also performed a numerical integration in Eq. (75) for an impurity-induced reduction of the staggered magnetization without x expansion. This yields the results pre-

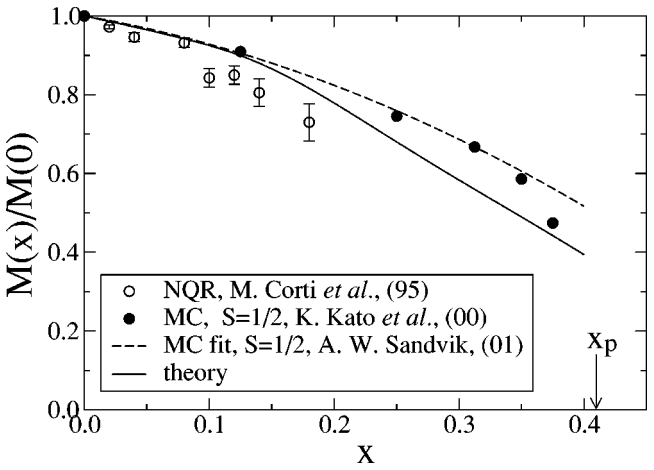

FIG. 10. Average staggered magnetization vs x. Our results from Eq. (75) (solid line), Monte Carlo data (open circles; Ref. 25), NQR data (filled circles; Ref. 56), and the fit of Monte Carlo data from Ref. 26 are shown.

sented in Fig. 10 for $S=1/2$ (solid line). Monte Carlo data from Ref. 25 (filled circles), and nuclear quadrupole resonance (NQR) data (open circles) from Ref. 56, are also shown. Note that the original Monte Carlo data of Ref. 25 are normalized by the total number of sites, while both NQR and our results are averaged over the magnetic sites only. In order to extract the same quantity from the Monte Carlo data, we divided them by the classical probability to find a spin-occupied site within the infinite cluster.[48] A recent Monte Carlo study Ref. 26 provided an analytical expression for the fit of the ''quantum-mechanical factor'' in the magnetization [see the comment after Eq. (74)] which we plot in Fig. 10 as well (dashed line). One can see a very good agreement of our results with numerical data up to high concentrations. The oxidation of the crystals can be the reason of a faster decrease of $M(x)$ in NQR data.

The absolute value of impurity-induced quantum fluctuations $\delta M(x)$ is independent of S in the linear spin-wave approximation similar to the quantum reduction of S by zero-point fluctuations Δ. We plot our results for $\delta M(x)$ in Fig. 11 in order to emphasize the agreement with the MC data for $S=1/2$ (circles) and $S=1$ (squares), which show only weak S dependences.

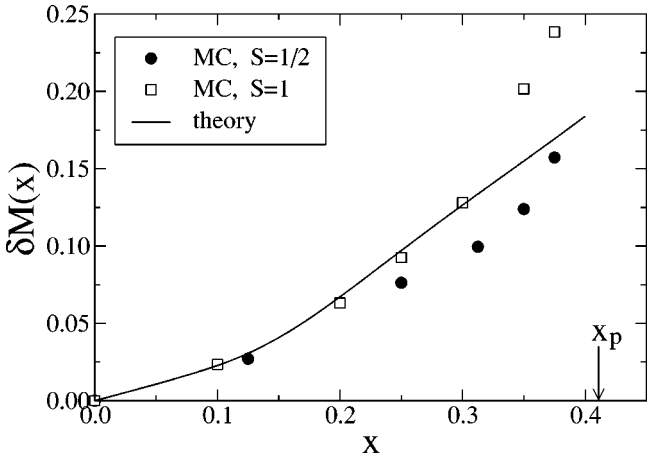

FIG. 11. The absolute value of $\delta M(x)$ from Eq. (75) (line) and Monte Carlo data Ref. 25, for $S=1/2$ (circles) and $S=1$ (squares).

It is worth mentioning here that discrete static quantities, zero-point spin deviations at the neighboring sites around impurities in an AF, were studied using spin-wave theory and Green's-function methods, since the 1960s (Refs. 57) with the most recent results obtained in Refs. 7 and 53. Quite remarkably, these results[53] were found to be in very good agreement with the recent Monte Carlo studies of a 2D $S=1/2$ Heisenberg model with impurities (Ref. 9). Note that while Refs. 53 and 57 focused on discrete quantities, our results concern averaged quantities.

At $T>0$, Eq. (74) for the staggered magnetic moment can be rewritten, separating the quantum ($T=0$), and thermal (T-dependent) parts,

$$M(x,T)=S-\Delta-\delta M(x)-\delta M^T(x,T), \tag{79}$$

$$\delta M^T(x,T)=\sum_{\mathbf{k}} \int_0^1 \frac{n_B(\omega)d\omega}{\omega_{\mathbf{k}}}[A_{\mathbf{k}}^{11}(\omega)+A_{\mathbf{k}}^{22}(\omega) - 2\gamma_{\mathbf{k}}A_{\mathbf{k}}^{12}(\omega)],$$

where $\delta M(x)$ is the zero-temperature part given in Eq. (75) and we used evident symmetries of the spectral functions with respect to $\omega\to-\omega$ and that $n_B(\omega)=-1-n_B(-\omega)$.

For a true 2D system at $x=0$ and $T>0$ thermal fluctuation destroy the LRO which manifests itself as a log divergency of the thermal correction to the magnetization,

$$\delta M^T(0,T)=\sum_{\mathbf{k}} \int_0^1 \frac{n_B(\omega)d\omega}{\omega_{\mathbf{k}}}\delta(\omega-\omega_{\mathbf{k}}) \simeq \frac{2}{\pi}\int_0^T \frac{Td\omega}{\omega}, \tag{80}$$

where $n_B(\omega)\simeq T/\omega$ at $T\ll\omega$. The 3D coupling provides a cut off to this divergency in a quasi-2D problem, which yields a finite value of the thermal correction:

$$\delta M^T(0,T)\simeq \frac{2}{\pi}\int_{\sqrt{4\tau}}^T n_B(\omega)d\omega\simeq \frac{2}{\pi}T\ln\left|\frac{T}{\sqrt{4\tau}}\right|. \tag{81}$$

In addition, a finite value of the Néel temperature, whose mean-field value can be found from the condition $M(0,T)=0=S-\Delta-\delta M^T(0,T)$, gives

$$T_N^{MF}\simeq\frac{\pi(S-\Delta)}{\ln\tau^{-1}}\ll 1; \tag{82}$$

in units of $4SJ$. T_N vanishes when $\tau\to 0$.

One would expect that the thermal part of the staggered magnetization for a diluted system may possess other divergences, stronger than the simple log-ω for the pure system. In fact, this suggestion is quite natural, since the spectrum is not linear, therefore, the nonlinear corrections must show themselves. Indeed, since the correction to the spectrum is $\delta\omega_{\mathbf{k}}\sim x\omega_{\mathbf{k}}\ln|\omega|$ [Eq. (51)], one immediately suggests that the thermal part of the magnetization should acquire a term

$$\sim xT\int \frac{\ln|\omega|d\omega}{\omega}\sim xT\ln^2|\omega|. \tag{83}$$

However, we show that such anomalous terms from diagonal and off-diagonal spectral functions cancel each other. As a result, there is no signature of any divergency in this quantity caused by the anomalies of the spectrum.

Using the x-expanded form for Green's functions (67) and (76) in the long-wavelength approximation, one finds the diagonal part

$$\begin{aligned}\delta M_d^T(x,T)&=\sum_{\mathbf{k}}\frac{1}{\omega_{\mathbf{k}}}\langle\alpha_{\mathbf{k}}^\dagger\alpha_{\mathbf{k}}\rangle^T\\&\simeq\sum_{\mathbf{k}}\int_0^1\frac{n_B(\omega)d\omega}{\pi\omega_{\mathbf{k}}}\left\{\pi\delta(\omega-\omega_{\mathbf{k}})\right.\\&\left.\times\left[1-\frac{\partial\mathrm{Re}\Sigma_{\mathbf{k}}(\omega_{\mathbf{k}})}{\partial\omega_{\mathbf{k}}}\right]-\frac{2x\omega_{\mathbf{k}}}{\omega^2-\omega_{\mathbf{k}}^2}\right\}\\&\simeq\frac{2}{\pi}\int_0^1 n_B(\omega)d\omega\left[1-x\left(2\rho'(\omega)-\frac{\pi}{2}+1-\frac{2}{\pi}\right)\right],\end{aligned} \tag{84}$$

and the off-diagonal part

$$\begin{aligned}\delta M_{od}^T(x,T)&=-\sum_{\mathbf{k}}\frac{\gamma_{\mathbf{k}}}{\omega_{\mathbf{k}}}\langle\alpha_{\mathbf{k}}^\dagger\beta_{\mathbf{k}}^\dagger\rangle^T\\&\simeq\sum_{\mathbf{k}}\int_0^1\frac{n_B(\omega)d\omega}{\pi\omega_{\mathbf{k}}}x\gamma_{\mathbf{k}}^2\left\{\pi\delta(\omega-\omega_{\mathbf{k}})\right.\\&\left.\times\left[\rho'(\omega_{\mathbf{k}})+\frac{\pi}{2}\right]+\frac{2\omega_{\mathbf{k}}}{\omega^2-\omega_{\mathbf{k}}^2}\right\}\\&\simeq\frac{2x}{\pi}\int_0^1 n_B(\omega)d\omega\left[2\rho'(\omega)+\frac{\pi}{2}+1\right]\end{aligned} \tag{85}$$

of the temperature-dependent $\delta M^T(x,T)$, where we kept only $O(\ln|\omega|)$ and $O(1)$ terms in the integrand. $\rho'(\omega)\equiv\mathrm{Re}\,\rho(\omega)$, integration by parts was used in δM_d^T and the, superscript T in the averages means the thermal part.

The total result is

$$\delta M^T(x,T)\simeq\left[1+x\left(\pi-\frac{2}{\pi}\right)\right]\delta M^T(0,T), \tag{86}$$

which shows that the thermal correction is enhanced by impurities, but that there is no new divergency associated with them in this quantity. The suppression rate of the Néel temperature can be readily obtained from the condition $M(x,T)=0=S-\Delta-\delta M(x)-\delta M(x,T)$ using Eq. (86) which gives

$$\frac{T_N(x)}{T_N(0)}\simeq 1-A_s x=1-x\left(\pi-\frac{2}{\pi}+\frac{B}{S-\Delta}\right). \tag{87}$$

For $S=1/2$ this gives $A_{1/2}=3.196(5)$, and for $S=5/2$ it is $A_{5/2}=2.600(4)$. It is important to note that these suppression rates point to $x_c(1/2)\simeq 0.31$ and $x_c(5/2)\simeq 0.38$, both below x_p, so that one may suggest that in order to have a phase transition at the classical percolation threshold the $T_N(x)/T_N(0)$ curves should have a rather unusual concave form.

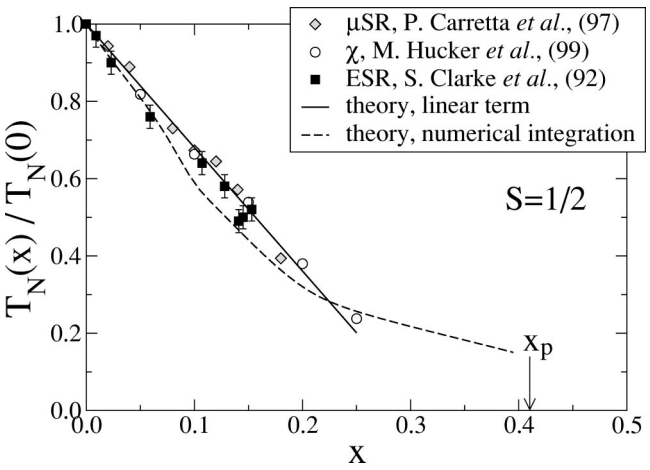

FIG. 12. $T_N(x)/T_N(0)$ vs x for $S=1/2$. Shown are the results of numerical integration in Eq. (74) (dashed line), the analytical linear-x slope $(1-A_{1/2}x)$ [Eq. (87)] (solid line), μSR (diamonds),[21] and magnetic susceptibility (circles)[19] data for Zn-doped LCO, and ESR (squares) (Ref. 22) of Zn-doped copper formate tetrahydrate $Cu_{1-x}Zn(Mg)_x(HCO_2)\cdot H_2O$.

It is interesting to compare our result for the decline rate of $T_N(x)$ [Eq. (87)] to the results of different approaches to the same problem and to the results for similar models. A naive mean-field treatment of the impurity effects as a simple renormalization of magnetic coupling gives $T_N(x)/T_N(0)=1-x$. The application of our formalism to the Ising limit of the 2D problem gives $T_N(x)/T_N(0)=1-A^I x$ with $A^I\simeq 1.37$ (see Appendix F) which is very close to the random-phase-approximation (RPA) answer $A^I_{RPA}=1.33$, and below the exact answer $A^I_{exact}\simeq 1.57$.[58] For 2D Ising magnets, $T_N(x)$ vs, x has a more traditional convex form.[17] The previous result for the suppression rate of T_N for a 2D Heisenberg model[59] is $T_N(x)/T_N(0)=1-\pi x$, which was obtained using the Green function technique and spin-wave theory in approximations very similar to ours. However, Ref. 59 missed $-2/\pi$, and neglected $1/S$ terms.

We have also performed a numerical integration in Eq. (74) and solved an implicit equation $M(x,T_N)=0$ on $T_N(x)$ numerically. This procedure requires a finite 3D coupling, and the use of a quasi-2D form of the spectral functions. Since the integration involves an additional dimension and the 3D region is quite narrow, the convergence of the result as a function of the number of $\mathbf{k}$, and ω points at small x can be an issue. We plot our numerical results for $T_N(x)/T_N(0)$ for the case of $S=1/2$ in Fig. 12, together with the analytical slope [Eq. (87)] with $A_{1/2}=3.2$ and experimental data. Experimental data are obtained by muon spin rotation (μSR) (Ref. 21) and magnetic susceptibility measurements[19] of LCO systems and by electron spin resonance (ESR) (Ref. 22) of Zn-doped copper formate tetrahydrate, a layered quasi-2D AF. One can see that our linear-x results agree very

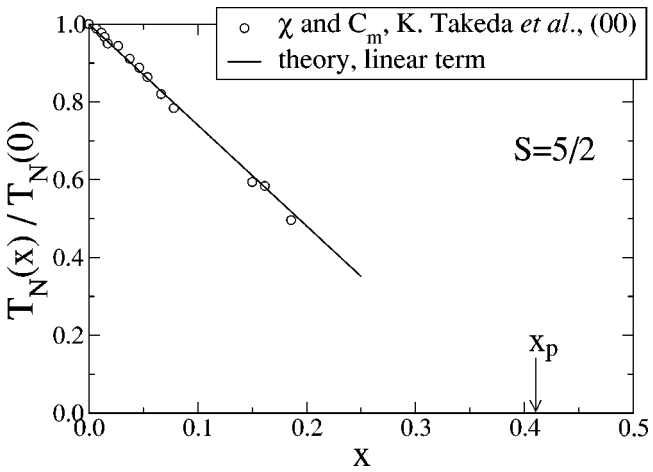

FIG. 13. $T_N(x)/T_N(0)$ vs x for $S=5/2$. Shown are analytical linear-x results $(1-A_{5/2}x)$ [Eq. (87)] (solid line), and results of magnetic susceptibility and specific-heat data for $Mn_{1-x}Zn(Mg,Cd)_x(HCO_2)_2 2(NH_2)_2CO$ (circles) (Ref. 24).

well with the experimental data up to a rather high doping level $x \approx 0.25$. There is a slight disagreement between our own numerical and linear-x analytical results at small x, which may be connected not only with the numerical accuracy but with the corrections of the order $\sim x T_N/J \sim x/\ln \tau^{-1}$. Note that the linear-$x$ result is free from such corrections, since it is obtained in the $\tau \to 0$ limit.

As discussed extensively in Ref. 60, the spin-wave theory for layered materials is not really adequate at $T \sim T_N$ due to the lack of kinematic constraints. When it is applied to the mean-field equation $M(x,T_N)=0$ it tends to overestimate the absolute value of the Néel temperature, and has some other artifacts such as $M(T) \sim T_N - T$ at $T \sim T_N$. This may also provide an additional x dependence in our numerical values of $T_N(x)/T_N(0)$.

Figures 13 shows our analytical slope for $T_N(x)/T_N(0)$ [Eq. (87)] with $A_{5/2}=2.6$ for the case of $S=5/2$, and experimental data from magnetic susceptibility and specific-heat measurements of $Mn_{1-x}Zn(Mg,Cd)_x(HCO_2)_2 2(NH_2)_2CO$, a layered $S=5/2$ material,[24]. One can see that while the scattering of experimental points seem to be smaller than in the $S=1/2$ case the linear-x result fits them very closely up to $x=0.2$. The older $T_N(x)/T_N(0)$ data for the more traditional $S=5/2$ material $K_2Mn_{1-x}Mg_xF_4$ (Ref. 29) showed a large scattering of the data, which allowed an almost any reasonable fit.[17]

It is worth mentioning that the numerical results of our approach for $T_N(x)$ bends inward at larger values of x, and show the above-mentioned concave form, which was recently observed experimentally for LCO compounds[18] and anticipated in other works.[24] While our approach is certainly not adequate at such high impurity concentrations, and tends to overestimate the value of $T_N(x)$ in comparison with experiments, it nevertheless points to the same physics. We interpret this behavior as due to localization effects, which tend to reduce the role of quantum and thermal fluctuations in the destruction of the long-range order.

In the paramagnetic phase above the Néel ordering temperature the 3D coupling is irrelevant, and the spin fluctuations in the layered AF system are characterized by an in-plane correlation length ξ_{2D} which is exponentially diverging with $1/T$ as $T \to 0$. The correlation length is uniquely determined by $T=0$ properties of the system such as the spin stiffness constant ρ_s.

The correlation length can be derived from the modified spin-wave theory, as suggested in Ref. 50, by introducing a chemical potential for magnons which produces a gap in the spin-wave dispersion, and then by resolving a constraint $\langle S_i^z \rangle = 0$ which defines the correlation length self-consistently. The result of such calculations at $x=0$ is[50]

$$\xi(T) \simeq \frac{c}{2T} \exp\left(\frac{2\pi\rho_s}{T}\right). \tag{88}$$

One should bear in mind, however, that while this approach gives the correct exponential behavior of $\xi_{2D}(T)$, it provides a prefactor equivalent to the one-loop renormalization-group result.[1,2] This prefactor must be modified according to the higher-order renormalization group treatment,[61] which gives[62]

$$\xi(T) \simeq \frac{e}{2} \frac{c}{4\pi\rho_s + T} \exp\left(\frac{2\pi\rho_s}{T}\right). \tag{89}$$

This expression shows an excellent agreement with experiments and Monte Carlo data.[3,21,63] This discrepancy between the results of modified spin-wave theory and the result of a more exact, nonperturbative, approach, is of the same origin as the overestimation of T_N by the mean-field solution of $\langle S_i^z \rangle = 0$.[60]

We generalize the approach of Ref. 50 for the case of an AF with impurities, and obtain, for the constraint,

$$S - \frac{1}{2}\sum_{\mathbf{k}} \left(\frac{1}{\omega_{\mathbf{k}}(\eta)} - 1 \right) = \sum_{\mathbf{k}} \frac{1}{\omega_{\mathbf{k}}(\eta)} [\langle \alpha_{\mathbf{k}}^\dagger \alpha_{\mathbf{k}} \rangle - \gamma_{\mathbf{k}} \langle \alpha_{\mathbf{k}}^\dagger \beta_{\mathbf{k}}^\dagger \rangle], \tag{90}$$

where $\omega_{\mathbf{k}}(\eta) = \sqrt{1-\eta^2\gamma_{\mathbf{k}}^2}$ and magnon averages are given by the integrals of the spectral functions $A_{\mathbf{k}}^{11}(\omega)$ and $A_{\mathbf{k}}^{12}(\omega)$ from Eqs. (40) and (41) in which the gapped form of the spin-wave spectrum is used.

We have performed a numerical integration in Eq. (90), and calculated the correlation length $\xi_{2D}(x,T) = \eta^2/\sqrt{8(1-\eta^2)}$ as a function of T for several values of x. We fit the results of such a numerical procedure in a wide temperature range almost exactly, with the help of the original Takahashi formula, [Eq. (88)], with the spin stiffness $\rho_s(x)$ being a free parameter. These fitting values of $\rho_s(x)/\rho_s(0)$ vs x closely follow our result for $T_N(x)/T_N(0)$ dependence [Fig. 12]. Such a result can be anticipated from a mean-field picture of the ordering in layered systems. The transition occurs when the interplane coupling is strong enough to stabilize the LRO in comparison with the thermal fluctuations: $J_\perp M^2(x) \xi^2[x,T_N(x)] \approx T_N$. If the correlation length preserves its exponential form, the dominant part of the left-hand side comes from $e^{2\pi\rho_s(x)/T_N(x)}$, and one immediately arrives at

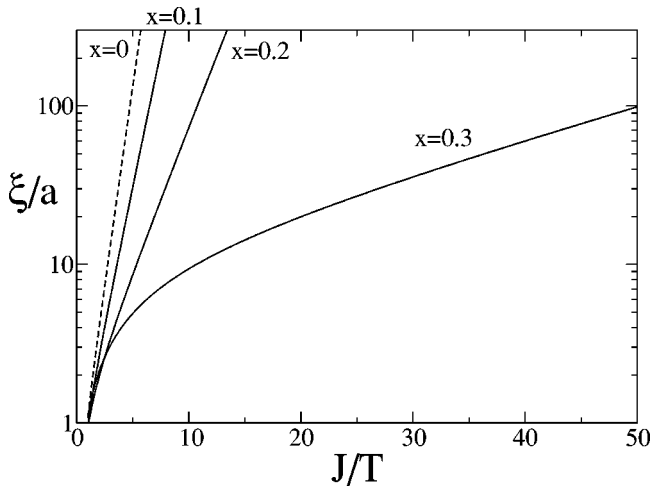

FIG. 14. $\xi(x,T)$ from Eq. (89), with $\rho_s(x)=\rho_s(0)(1-A_{1/2}x)$ from Eq. (87), vs J/T for $x=0$ (dashed line), $x=0.1$, $x=0.2$, and $x=0.3$ (solid lines).

$$\frac{\rho_s(x)}{\rho_s(0)}=\frac{T_N(x)}{T_N(0)}+O(x/\ln\tau^{-1}). \tag{91}$$

Therefore, the important conclusions one can make from our analysis is that (i) the correlation length should follow the $x=0$ type of behavior Eq. (89) with x-dependent ρ_s, at least for not too low T and not too high x, and (ii) $\rho_s(x)/\rho_s(0) \simeq T_N(x)/T_N(0)$.

Figure 14 shows a semilog plot of $\xi(x,T)$ given by formula in Eq. (89) with $\rho_s(x)=\rho_s(0)(1-A_{1/2}x)$,$A_{1/2}$ is from Eq. (87), vs J/T for $x=0$ (dashed line), $x=0.1$, $x=0.2$, and $x=0.3$ (solid lines). An important observation can be made here. At small x $2\pi\rho_s$ is of the order of J, and at all reasonable temperatures the dominant behavior is exponential in J/T (straight line in the semilog scale). When the spin stiffness becomes small ($\rho_s \ll J$), there is an additional temperature range $J \gg T \gg \rho_s$ where the exponential behavior is not seen while the prefactor gives the $\log(J/T)$ behavior of the $\log(\xi)$ clearly seen for $x=0.3$. The experimentally observed deviation from the simple exponential behavior of the correlation length $\xi(T,x)$ vs $1/T$[18] can be related to this effect.

At a larger doping level close to the percolation threshold, one expects another length-scale to appear. This length scale is associated with crossover from translational invariance to self-similarity in the percolative systems.[64] Below x_p the ''geometrical length'' $\xi_G \propto |x-x_p|^{-\nu}$ separates the regions of Euclidean and fractal geometries. Above x_p, where no infinite clusters are left, ξ_G is the characteristic size of the finite clusters. Earlier experimental studies of 2D and 3D Ising systems ($Rb_2Co_xMg_{1-x}F_4$ and $Fe_{1-x}Zn_xF_2$)[65,66] and near-Heisenberg systems ($Rb_2Mn_xMg_{1-x}F_4$ and $Mn_{1-x}Zn_xF_2$) (Ref. 67 and 68) systems, close to x_p, demonstrated that the static structure factor $\mathcal{S}(\mathbf{q})$ contains contributions from both ''thermal'' and ''geometrical'' lengths in agreement with the theoretical studies.[32,69] The experimental data suggest that these lengths combine in the simplest possible form $\xi^{-1}=\xi^{-1}(T)+\xi_G^{-1}(x)$, and that the Lorentzian form of the structure factor near ordering vector is preserved. Yet another interesting result of the proximity to the percolation is that, at $x<x_p$ below T_N, the elastic Bragg peak should be accompanied by the Lorentzian whose width at $T=0$ is solely defined by the inverse ''geometrical length'' ξ_G^{-1}. One would expect similar effects to be observed in newly available LCO systems close to x_p.[18]

It is not clear, whether localization effects in an infinite cluster, which we discuss in this work, can manifest themselves in the static structure factor or correlation length. Such contributions, if they exist, may lead to an interesting behavior of the correlation length, different from the simple renormalization of spin stiffness. However, in our approach the potential sources of such anomalous terms appear at higher order in $x(\sim x^2)$ and, most certainly, do not affect the results for the experimentally reachable domain of lengths $\xi \lesssim 200a$ above which the ordering occurs. At larger concentrations x, such contributions can become important for shorter correlation lengths, but in reality they might be screened by similar effects from the decoupled clusters.

Theoretically, it is very intriguing whether such localization effects of the infinite cluster can really affect the behavior of correlation length. We reserve this subject for further study.

V. CONCLUSIONS

We have studied the problem of diluted 2D and quasi-2D quantum Heisenberg antiferromagnets in a tetragonal lattice, making use of linear spin-wave theory and T-matrix approach. We have shown, contrary to earlier findings, that $D=2$ is *not* the lower critical dimension for this kind of disorder, and that at $T=0$ long-range order persists up to concentrations close to the classical percolation threshold. These results are consistent with Monte Carlo simulations in large lattices.[25] In agreement with earlier works on this subject, which studied the problem in the leading order of the dilution fraction x,[30,37] we found that the spin-wave spectrum is strongly modified by disorder. However, contrary to these works, we have shown that this result does *not* imply an instability of the system to a paramagnetic phase. Rather, it indicates magnon localization on a length scale l, exponentially large in $1/x$. We have shown that this length scale appears explicitly in the dynamic properties such as the dynamical structure factor $\mathcal{S}(\mathbf{k},\omega)$ [Eqs. (57)–(65)], which can be measured directly in neutron-scattering experiments, and the magnon density of states $N(\omega)$ [Eqs. (68) and (69)] which is directly related to the magnetic specific heat equations (70) and (71). The measurement of such quantities will provide a direct test of our theory. Furthermore, we show that the static properties such as the zero-temperature staggered magnetization $M(x)$ [Eq. (74)] and Néel temperature $T_N(x)$ (in the quasi-2D case) do not show any anomaly associated with the spectrum and are finite up to the concentration close to the classical percolation threshold. These results are in a quantitative agreement with the NQR,[56] μSR,[20] ESR,[22] and magnetic susceptibility[19] measurements in different compounds, as well as with the Monte Carlo data.[25]

We have shown that the effect of dilution of an AF with

nonmagnetic impurities is quite strong, because dilution completely removes spin degrees of freedom from the impurity site; therefore, the spin waves are strongly scattered. Moreover, the low dimensionality of the system significantly constrains the phase space for scattering, leading to localization effects. We have shown that a hydrodynamic description of the problem breaks down for length scales larger than l and that the spin excitations become diffusive instead of ballistic. The conventional averaging procedure which is used to treat disorder does not lead to an effective medium with renormalized parameters. Therefore, one needs to use a different approach for length scales larger than l, a problem which is beyond the scope of this paper.

In fact, the physics of localization described in our work has similarities to the Anderson localization for noninteracting electrons in disordered lattices where the statistics of the excitations does not matter.[70] Note that our problem should be close to the problem of localization of relativistic bosons (with chemical potential $\mu=0$) in a random potential. On the other hand, that problem is related to the problem of disorder in Bose-Hubbard model where nonrelativistic bosons with kinetic energy J interact through the local Coulomb term U.[71] In the latter model the Bose glass phase appears for small J at a zero chemical potential, and transition into a superfluid state is possible when J is large enough. In our case superfluidity is not possible, but we may conjecture that our localized phase is somewhat similar to the Bose glass phase, and that magnons are trapped in the regions which are more ordered than in average. It is not clear, however, if the relativistic nature of the bosons is important for the nature of localization.

Furthermore, we find the close similarity of our problem to the problem of disorder in 2D d-wave superconductors.[44,52] The large enhancement of the density of states at low frequencies in our case, which comes about because of the redistribution of spectral weight over the entire Brillouin zone, is reminiscent of that problem. In d-wave superconductors the elementary excitations are nodal quasiparticles, or relativistic (Dirac) fermions. It is known that for these excitations localization occurs on a length scale l_L (localization length) which is an exponential function of the conductance σ: $l_L \propto e^{\sigma/\sigma_0}$,[72] where $\sigma_0 = e^2/h$. Since in the dilute limit one expects the conductance to diverge with x (that is, $\sigma \propto 1/x$) the localization length has the same type of nonanalytical dependence on x as in our case. However, it is not clear how (if possible) the two problems map onto each other. A further investigation, beyond the scope of this paper, can clarify the connection of the diluted antiferromagnet with other similar problems of disorder in low-dimensional systems.

In summary, we have presented a comprehensive study of diluted quantum Heisenberg antiferromagnets in 2D and quasi-2D systems. We have shown that while the dynamic properties possess anomalies associated with magnon localization, the static properties are free from such anomalies. Thus in low-dimensional systems with disorder, the connection between static and dynamic quantities is not straightforward. We have compared our results to the numerical simulations and experimental data with a very good agreement. We have also proposed other experiments which can further test the results of our theory. Altogether this provides a self-consistent picture of the effects of disorder in low-dimensional quantum antiferromagnets.

ACKNOWLEDGMENTS

We would like to acknowledge invaluable conversations with A. Abanov, A. Balatsky, A. Bishop, P. Carretta, C. Chamon, A. Chubukov, R. Fishman, B. Harris, A. Harrison, I. Gruzberg, M. Greven, M. Katsnelson, B. Keimer, H. Mook, D. Mandrus, S. Nagler, N. Nagaosa, L. Pryadko, S. Sachdev, A. Sandvik, O. Starykh, O. Sushkov, K. Takeda, S. Todo, O. Vajk, G. Vignale, and M. Zhitomirsky. This research was supported in part by Oak Ridge National Laboratory, managed by UT-Battelle, LLC, for the U.S. Department of Energy under Contract No. DE-AC05-00OR22725, and by a CULAR research grant under the auspices of the U.S. Department of Energy.

APPENDIX A: TETRAGONAL LATTICE GROUP THEORY

We first resolve the scattering potential $\hat{V}$ [Eqs. (9) and (10)] in $\mathbf{r}$-space by inserting the closure relation[73]

$$\hat{V}_{\mathbf{k}_1,\mathbf{k}_2} = \int d\mathbf{r}_1 \int d\mathbf{r}_2 \phi^*_{\mathbf{k}_1}(\mathbf{r}_1)\hat{V}_{\mathbf{r}_1,\mathbf{r}_2}\phi_{\mathbf{k}_2}(\mathbf{r}_2) = \int d\mathbf{r}_1 \int d\mathbf{r}_2 \phi^*_{\mathbf{k}_1}(\mathbf{r}_1) U_i^{\dagger}\hat{V}_{\mathbf{r}_1,\mathbf{r}_2} U_i \phi_{\mathbf{k}_2}(\mathbf{r}_2), \tag{A1}$$

where U_i is any symmetric operator in the group of tetragonal symmetry, and $\phi_{\mathbf{k}}(\mathbf{r})$ is a plane-wave function, $\phi_{\mathbf{k}}(\mathbf{r}) = (2\pi)^{3/2} e^{i\mathbf{k}\cdot\mathbf{r}}$, which can be decomposed by projection operators:

$$\phi_{\mathbf{k}}(\mathbf{r}) = \sum_p \sum_{n=1}^{l_p} \phi_{\mathbf{k}}(\mathbf{r})^{(p)}_n, \tag{A2}$$

where

$$\phi_{\mathbf{k}}(\mathbf{r})^{(p)}_n = \frac{l_p}{g} \sum_{i=1}^{16} D^{(p)}(U_i)_{nn} U_i \phi_{\mathbf{k}}(\mathbf{r}), \tag{A3}$$

where the set of functions, $\{\phi_{\mathbf{k}}(\mathbf{r})^{(p)}_n\}_{n=1,\ldots,l_p}$, form a basis of the pth irreducible representation, and l_p is the dimension of the pth irreducible representation; $D^{(p)}(U_i)_{nn}$ is the diagonal matrix elements of the pth irreducible representation for the symmetric operator U_i in point group D_{4h} whose order is $g(=16)$. We readily project the potential into irreducible representations as $\hat{V}_{\mathbf{k}_1,\mathbf{k}_2} = \Sigma_p \hat{V}^{(p)}_{\mathbf{k}_1,\mathbf{k}_2}$, where

$$\hat{V}^{(p)}_{\mathbf{k}_1,\mathbf{k}_2} = \sum_{n=1}^{l_p} \sum_{i,j=1}^{g} \frac{l_p^2}{g^2} D^{(p)}(U_i)_{nn} D^{(p)}(U_j)_{nn} \times \int d\mathbf{k}_3 \int d\mathbf{k}_4 A^i_{\mathbf{k}_1,\mathbf{k}_3} \hat{V}_{\mathbf{k}_3,\mathbf{k}_4} A^j_{\mathbf{k}_4,\mathbf{k}_2}, \tag{A4}$$

where

$$A^{i}_{\mathbf{k}_1,\mathbf{k}_2}=\int d\mathbf{r}\phi^{*}_{\mathbf{k}_1}(\mathbf{r})U_i\phi_{\mathbf{k}_2}(\mathbf{r}). \tag{A5}$$

Using the tetragonal symmetry group, one notes that each $A^{i}_{\mathbf{k}_1,\mathbf{k}_2}$ is a δ function. Thus the scattering potential $\hat{V}^{A}_{\mathbf{k}_1,\mathbf{k}_2}$ [Eq. (9)] can be decomposed into channels of irreducible representations. The nonzero orthogonal channels are (before the Bogolyubov transformation)

A_{1g} (s wave),

$$\hat{V}^{A,s}_{\mathbf{k}_1,\mathbf{k}_2}=|\mathrm{s}_{\mathbf{k}_1}\rangle\otimes\langle\mathrm{s}_{\mathbf{k}_2}|+|\mathrm{s}^{\perp}_{\mathbf{k}_1}\rangle\otimes\langle\mathrm{s}^{\perp}_{\mathbf{k}_2}|, \tag{A6}$$

E_u (in-plane p waves),

$$\hat{V}^{A,p_{x(y)}}_{\mathbf{k}_1,\mathbf{k}_2}=|\mathrm{p}^{x(y)}_{\mathbf{k}_1}\rangle\otimes\langle\mathrm{p}^{x(y)}_{\mathbf{k}_2}|, \tag{A7}$$

B_{1g} (d wave),

$$\hat{V}^{A,d}_{\mathbf{k}_1,\mathbf{k}_2}=|\mathrm{d}_{\mathbf{k}_1}\rangle\otimes\langle\mathrm{d}_{\mathbf{k}_2}|, \tag{A8}$$

and A_{2u} (p_z wave),

$$\hat{V}^{A,p_z}_{\mathbf{k}_1,\mathbf{k}_2}=|\mathrm{p}^{z}_{\mathbf{k}_1}\rangle\otimes\langle\mathrm{p}^{z}_{\mathbf{k}_2}|, \tag{A9}$$

where $\langle\mathrm{s}_{\mathbf{k}}|=[1,\gamma_{\mathbf{k}}]$, $\langle\mathrm{s}^{\perp}_{\mathbf{k}}|=\sqrt{\tau}[1,\gamma^{\perp}_{\mathbf{k}}]$, $\langle\mathrm{p}^{x(y)}_{\mathbf{k}}|=[0,1]\sin k_{x(y)}/\sqrt{2}$, $\langle\mathrm{d}_{\mathbf{k}}|=[0,1]\gamma^{-}_{\mathbf{k}}$ and $\langle\mathrm{p}^{z}_{\mathbf{k}}|=\sqrt{\tau}\sin k_z[0,1]/\sqrt{2}$. A Bogoliubov transformation yields Eqs. (18)–(21).

APPENDIX B: 3D *T* MATRIX

In this appendix we provide the solution of the s-wave T-matrix equation in the tetragonal lattice for the arbitrary relative value of the inter-plane and in-plane exchange integrals $\tau=J_{\perp}/2J$. With this solution we demonstrate the smallness of the 3D corrections to the 2D result in the quasi-2D case ($\tau\ll 1$).

After some algebra one can solve the T-matrix equation (25) with the s-wave scattering potential from Eq. (18) (sublattice A), $u_{\mathbf{k}}$, $v_{\mathbf{k}}$, and $\omega_{\mathbf{k}}$ from Eqs. (12) and (13), and obtain:

$$\hat{T}^{A,s}_{\mathbf{k},\mathbf{k}'}(\omega)=|s_{\mathbf{k}}\rangle\otimes\langle s_{\mathbf{k}'}|\cdot\Gamma_1(\omega)+|s^{\perp}_{\mathbf{k}}\rangle\otimes\langle s^{\perp}_{\mathbf{k}'}|\cdot\Gamma_2(\omega)+(|s_{\mathbf{k}}\rangle \otimes\langle s^{\perp}_{\mathbf{k}'}|+|s^{\perp}_{\mathbf{k}}\rangle\otimes\langle s_{\mathbf{k}'}|)\cdot\Gamma_3(\omega) \tag{B1}$$

where the ω dependence of the in-plane scattering (first term) is given by an expression which is formally similar to the pure 2D result [Eq. (28)],

$$\Gamma_1(\omega)=\frac{1}{\omega}+\frac{(1+\omega)\rho(\omega)+\tau R_1(\omega)}{1-\omega(1+\omega)\rho(\omega)+\tau D(\omega)}, \tag{B2}$$

with $\rho(\omega)$ given by Eq. (29). Note that the integration over $\mathbf{p}$ in this case is three dimensional. The inter plane scattering is

$$\Gamma_2(\omega)=-\tau+\frac{\tau^2}{\omega}-\frac{\tau^2R_2(\omega)}{1-\omega(1+\omega)\rho(\omega)+\tau D(\omega)}. \tag{B3}$$

The ω dependence of the cross-term is given by

$$\Gamma_3(\omega)=\frac{\tau}{\omega}+\frac{\tau R_3(\omega)}{1-\omega(1+\omega)\rho(\omega)+\tau D(\omega)}. \tag{B4}$$

All three parts of the scattering matrix possess the same "unphysical" $1/\omega$ contribution discussed in the text. Application of the projection procedure [Eqs. (30) and (31)] to this problem is beyond of the scope of this appendix.

The auxiliary functions D and R_i are given by rather cumbersome combinations of $\omega,\rho(\omega)$, and two additional integrals

$$\alpha(\omega)=\sum_{\mathbf{p}}\frac{(\gamma^{\perp}_{\mathbf{p}})^2}{\omega^2-\omega^2_{\mathbf{p}}},\qquad \beta(\omega)=\sum_{\mathbf{p}}\frac{\hat{\gamma}_{\mathbf{p}}\gamma^{\perp}_{\mathbf{p}}}{\omega^2-\omega^2_{\mathbf{p}}}, \tag{B5}$$

with $\hat{\gamma}_{\mathbf{p}}$, $\gamma^{\perp}_{\mathbf{p}}$, and $\omega_{\mathbf{p}}$ from Eqs. (5) and (13). Note that at $\tau\to 0$ $\alpha(\omega)\to\rho(\omega)/2$ and $\beta(\omega)\to 0$.

The expressions for D and R_i are

$$\begin{aligned} D&=P-\omega P_2,\\ R_1&=\rho-\alpha+P_2,\\ R_2&=\alpha-(\omega-\tau)P_2,\\ R_3&=(\rho+\alpha-P)/2+\tau(\rho-\alpha)/2+P_2, \end{aligned} \tag{B6}$$

where the following shorthand notations are used:

$$\begin{aligned} P&=\hat{\gamma}_0(\rho+\alpha)-2\beta,\\ P_2&=\hat{\gamma}^2_0\rho\alpha-\beta^2+\alpha-\omega P-\omega^2\rho\alpha. \end{aligned} \tag{B7}$$

There is no assumption about the value of τ made in these formulas.

At $\tau\ll 1$ and $\omega\ll 1$ (ω can be still $\gg\tau$) one can show that

$$\begin{aligned} D&\simeq 3\rho/2,\qquad R_1\simeq\rho^2/2+\rho,\\ R_2&\simeq\rho/2,\qquad R_3=O(\tau\rho^2). \end{aligned} \tag{B8}$$

In the same limit $\tau\ll 1$ and $\omega\ll 1$ the ω-dependent parts of the scattering matrix become (we simply omit the unphysical $1/\omega$ terms here)

$$\begin{aligned} \Gamma_1(\omega)&\simeq\rho-\tau(\rho^2-\rho),\\ \Gamma_2(\omega)&\simeq-\tau+\tau^2\rho/2,\\ \Gamma_3(\omega)&=O(\tau^2\rho^2). \end{aligned} \tag{B9}$$

Recall that in two dimensions $\Gamma_1(\omega)\simeq\rho$ and $\Gamma_2(\omega)=\Gamma_3(\omega)\equiv 0$. Since $\mathrm{Re}\,\rho\sim\ln|\omega|$ at $\omega\gg\sqrt{\tau}$ and $\mathrm{Re}\,\rho\sim\ln|\tau|$ at $\omega\ll\sqrt{4\tau}$ the largest relative correction to the 2D terms in the scattering matrix is $O[\tau\ln(\tau)]$. The same statement can be proved for all higher powers of ω in Eq. (B2), without assuming that $\omega\ll 1$.

The conclusion is, once again, that at $\tau\ll 1$ one can safely drop all terms explicitly proportional to τ in Eqs. (B2)–(B4), and thus arrive at the purely 2D expression for the scattering matrix given in Eq. (28). The only modification in the quasi-2D case versus 2D case is the change of the behavior

of $\rho(\omega)$ at low ω, whose real part saturates at $\omega \leqslant \sqrt{4\tau}$, and whose imaginary part acquires an extra power in ω (see Appendix E).

APPENDIX C: ELLIPTIC INTEGRALS

The energy-dependent part of the T-matrix equations (28) and (28) is expressed through the integrals of the Green's function [Eq. (29)]. These integrals can be evaluated in the case of a 2D system and are given by combinations of complete elliptic integrals of first and second kinds:

$$\rho(\omega)=\sum_{\mathbf{p}} \frac{1}{\omega^2-\omega_{\mathbf{p}}^2}=-\frac{2}{\pi\omega'}[K(\omega')+iK(\omega)], \quad \text{(C1)}$$

$$\rho_d(\omega)=\sum_{\mathbf{p}} \frac{(\gamma_{\mathbf{p}}^-)^2}{\omega^2-\omega_{\mathbf{p}}^2}$$

$$=1+\frac{2}{\pi\omega'}\{\omega^2 K(\omega')-2E(\omega')+i[(\omega^2-2)K(\omega)+E(\omega)]\},$$

where $\omega'=\sqrt{1-\omega^2}$, K and E are the complete elliptic integrals of the first and second kinds, respectively.[74]

In the low-energy limit

$$\rho(\omega)=\frac{2}{\pi}\ln|\omega/4|-i, \quad \text{(C2)}$$

$$\rho_d(\omega)=1-\frac{4}{\pi}. \quad \text{(C3)}$$

APPENDIX D: PROJECTION OF UNPHYSICAL STATES

After the introduction of a fictitious magnetic field to project out the unphysical on-site mode the s-wave scattering potential (sublattice A) is given by the sum of two terms from Eqs. (22) and (31):

$$\hat{V}_{\mathbf{k},\mathbf{k}'}^{A,s,total}=-|s_{\mathbf{k}}\rangle\otimes\langle s_{\mathbf{k}'}|+H_z|\Delta s_{\mathbf{k}}\rangle\otimes\langle\Delta s_{\mathbf{k}'}|,$$

with

$$\langle s_{\mathbf{k}}|=\omega_{\mathbf{k}}[u_{\mathbf{k}},-v_{\mathbf{k}}], \qquad \langle\Delta s_{\mathbf{k}}|=[u_{\mathbf{k}},v_{\mathbf{k}}]. \quad \text{(D1)}$$

One immediately suggest the form of the solution of the T-matrix equation:

$$\hat{T}_{\mathbf{k},\mathbf{k}'}^{A,s}(\omega)=|s_{\mathbf{k}}\rangle\otimes\langle s_{\mathbf{k}'}|\cdot\Gamma_1(\omega)+|\Delta s_{\mathbf{k}}\rangle\otimes\langle\Delta s_{\mathbf{k}'}|\cdot\Gamma_2(\omega)+(|\Delta s_{\mathbf{k}}\rangle\otimes\langle s_{\mathbf{k}'}|+|s_{\mathbf{k}}\rangle\otimes\langle\Delta s_{\mathbf{k}'}|)\cdot\Gamma_3(\omega). \quad \text{(D2)}$$

after some algebra, one finds

$$\Gamma_1(\omega)=\frac{H_z(1+\omega)\rho(\omega)+1}{[1-\omega(1+\omega)\rho(\omega)](H_z-\omega)},$$

$$\Gamma_2(\omega)=-\frac{\omega H_z}{H_z-\omega}, \quad \text{(D3)}$$

$$\Gamma_3(\omega)=\frac{H_z}{H_z-\omega},$$

which yield the answer given in Eqs. (32)–(34) in the limit $H_z\to\infty$.

APPENDIX E: 3D $\rho(\omega)$

The key ingredient of the low-energy T-matrix scattering is given by the integral of the Green's function over $\mathbf{k}$, $\rho(\omega)$ [Eq. (29)]. Appendix C gives an analytical expression of $\rho(\omega)$ in the 2D case. In the quasi-2D case the interplane coupling provides a cutoff in the logarithm, and gives an extra power of ω in the imaginary part of the integral in the 3D energy range. This can be obtained explicitly using 3D form of the spin-wave dispersion [Eq. (13)] $\omega_{\mathbf{k}}=\sqrt{\hat{\gamma}_0^2-\hat{\gamma}_{\mathbf{k}}^2}$.

In the limits $\sqrt{\tau}=\sqrt{J_\perp/2J}\ll 1$ and $\omega\ll 1$ (for arbitrary $\omega/\sqrt{\tau}$), for the real part of $\rho(\omega)$ one obtains

$$\mathrm{Re}\,\rho(\omega)=\frac{2}{\pi}\ln\left|\frac{\sqrt{\tau}}{4}\right|+O(\tau,\omega^2), \quad \text{for} \quad \omega\leqslant\sqrt{4\tau}$$

$$\mathrm{Re}\rho(\omega)=\frac{2}{\pi}\ln\left|\frac{\omega+\sqrt{\omega^2-4\tau}}{8}\right|+O(\tau,\omega^2), \quad \text{for} \quad \omega\geqslant\sqrt{4\tau}, \quad \text{(E1)}$$

at $\omega\gg\sqrt{4\tau}$ the 3D energy scale is irrelevant, and $\mathrm{Re}\rho(\omega)=2/\pi\ln|\omega/4|$ is back to its 2D form. The imaginary parts of $\rho(\omega)$ is

$$\mathrm{Im}\,\rho(\omega)=-\frac{1}{\pi}\arccos\left(\frac{\sqrt{(1+\tau)^2-\omega^2}-1}{\tau}\right)+O(\omega^2)$$

$$=-\frac{1}{\pi}\arccos\left(1-\frac{\omega^2}{2\tau}\right)+O(\tau^2,\omega^2)$$

$$\text{for} \quad \omega\leqslant\sqrt{4\tau}, \quad \text{(E2)}$$

$$\mathrm{Im}\,\rho(\omega)=-1+O(\omega^2), \quad \text{for} \quad \omega\geqslant\sqrt{4\tau}.$$

At small $\omega\ll\sqrt{4\tau}$ deep in the 3D range of energies, $\mathrm{Im}\,\rho(\omega)=-\omega/\pi\sqrt{\tau}$ is linear in ω.

APPENDIX F: $T_N(x)$ FOR THE ISING PROBLEM

In this appendix we apply the formalism of our work to the problem of $T_N(x)$ vs x dependence for the Ising $S=1/2$ case. While the spin-wave approximation is much less adequate in the Ising limit than for the pure Heisenberg model, it is nevertheless a very instructive exercise which gives a quantitatively correct answer.

The quadratic part of the 2D $S=1/2$ Ising model in the spin-wave approximation reads

$$\frac{\mathcal{H}}{2J} = \mathcal{H}_0 + \mathcal{H}_{imp}$$

$$= \sum_{\mathbf{k}} a^{\dagger}_{\mathbf{k}} a_{\mathbf{k}} - \sum_{l,\mathbf{k},\mathbf{k}'} e^{i(\mathbf{k}-\mathbf{k}')\mathbf{R}_l} V_{\mathbf{k},\mathbf{k}'} a^{\dagger}_{\mathbf{k}} a_{\mathbf{k}'}, \qquad \text{(F1)}$$

with

$$V_{\mathbf{k},\mathbf{k}'} = \gamma_{\mathbf{k}-\mathbf{k}'}, \qquad \text{(F2)}$$

where from the beginning we omit the ''unphysical'' term which will result in a $\omega = 0$ mode. The T matrix gives the total result for all scattering channels,

$$T^{tot}_{\mathbf{k},\mathbf{k}'}(\omega) = -\gamma_{\mathbf{k}-\mathbf{k}'} \frac{\omega - 1}{\omega - 3/4}, \qquad \text{(F3)}$$

where we used the property

$$\sum_{\mathbf{p}} \gamma_{\mathbf{k}-\mathbf{p}} \gamma_{\mathbf{p}-\mathbf{k}'} \equiv \gamma_{\mathbf{k}-\mathbf{k}'}/4. \qquad \text{(F4)}$$

The self-energy is then given by

$$\Sigma(\omega) = -x \frac{\omega - 1}{\omega - 3/4}. \qquad \text{(F5)}$$

The Green's function has now two poles:

$$G(\omega) = \frac{1}{\omega - 1} \cdot \frac{\omega - 3/4}{\omega - 3/4 + x}, \qquad \text{(F6)}$$

and the spectral function is given by two δ peaks:

$$A(\omega) = \frac{1}{1+4x}[\delta(\omega - 1) + 4x\,\delta(\omega - 3/4 + x)]. \qquad \text{(F7)}$$

The Néel temperature is defined from the condition

$$\langle S^z \rangle (T_N, x) = \frac{1}{2} - \int_{-\infty}^{\infty} d\omega\, n_B(\omega) A(\omega) = 0, \qquad \text{(F8)}$$

which transforms to

$$\frac{1+4x}{2} = n_B(1) + 4x\, n_B(3/4 - x). \qquad \text{(F9)}$$

In a pure system $T_N(0)/2J = 1/\ln 3$. At small $xT_N(x) \simeq T_N(0)(1 - A^I x)$ and, after some algebra, one obtains an analytical expression for A^I,

$$A^I = \frac{4}{3}\frac{2}{\ln 3}\left[\frac{2}{3^{3/4} - 1} - 1\right] \simeq 1.025\frac{4}{3} \simeq 1.37, \qquad \text{(F10)}$$

which should be compared with the RPA answer $A^I_{RPA} = 4/3$[59] and an exact answer $A^I_{exact} \simeq 1.57$.[58] One can see that in spite of the roughness of the approximation of the Ising spin degrees of freedom by bosons, our approach gives a good quantitative agreement with other approaches and with an exact result.

*Also at the Institute of Semiconductor Physics, Novosibirsk, Russia.

†On leave from Department of Physics, University of California, Riverside.

[1] S. Chakravarty, B.I. Halperin, and S.B. Nelson, Phys. Rev. Lett. **60**, 1057 (1988); Phys. Rev. B **39**, 2344 (1989).

[2] E. Manousakis, Rev. Mod. Phys. **63**, 1 (1991).

[3] M.A. Kastner, R.J. Birgeneau, G. Shirane, and Y. Endoh, Rev. Mod. Phys. **70**, 897 (1998).

[4] R.R.P. Singh, W.E. Pickett, D.W. Hone, and D.J. Scalapino, Comments Mod. Phys. **2**, B1 (2000); cond-mat/0007086 (unpublished).

[5] P. Sen and A. Singh, Phys. Rev. B **53**, 328 (1996); **53**, 6406 (1996); P. Sen, S. Basu, and A. Singh, *ibid.* **50**, 10 381 (1994); P. Sen, Int. J. Mod. Phys. B **13**, 3193 (1999).

[6] N. Nagaosa, A. Furusaki, M. Sigrist, and H. Fukuyama, J. Phys. Soc. Jpn. **65**, 3724 (1996).

[7] A.G. Malshukov and G.D. Mahan, Phys. Rev. Lett. **68**, 2200 (1992).

[8] V.Yu. Irkhin, A.A. Katanin, and M.I. Katsnelson, Phys. Rev. B **60**, 14 779 (1999).

[9] A.W. Sandvik, E. Dagotto, and D.J. Scalapino, Phys. Rev. B **56**, 11 701 (1997).

[10] A.W. Sandvik and M. Vekic, Phys. Rev. Lett. **74**, 1226 (1995).

[11] V.N. Kotov, J. Oitmaa, and O. Sushkov, Phys. Rev. B **58**, 8495 (1998).

[12] T.-K. Ng, Phys. Rev. B **54**, 11 921 (1996).

[13] D.G. Clarke, T. Giamarchi, and B. Shraiman, Phys. Rev. B **48**, 7070 (1993).

[14] J. Oitmaa, D.D. Betts, and M. Audin, Phys. Rev. B **51**, 2896 (1995).

[15] W. Brenig and A.P. Kampf, Phys. Rev. B **43**, 12 914 (1991).

[16] C. Yasuda, and A. Oguchi, J. Phys. Soc. Jpn. **68**, 2773 (1999).

[17] S-W. Cheong, A.S. Cooper, L.W. Rupp, Jr., B. Batlogg, J.D. Thompson, and Z. Fisk, Phys. Rev. B **44**, R9739 (1991).

[18] O.P. Vajk, P.K. Mang, M. Greven, P.M. Gehring, and J.W. Lynn (unpublished).

[19] M. Hücker, V. Kataev, J. Pommer, J. Harraß, A. Hosni, C. Pflitsch, R. Gross, and B. Büchner, Phys. Rev. B **59**, R725 (1999).

[20] P. Carretta, A. Rigamonti, and R. Sala, Phys. Rev. B **55**, 3734 (1997).

[21] Copper formate tetradeuterate $Cu(HCO_2)D_2O$, $S = 1/2$; see H.M. Ronnow, D.F. McMorrow, and A. Harrison, Phys. Rev. Lett. **82**, 3152 (1999); P. Carretta, T. Ciabattoni, A. Cuccoli, E. Mognaschi, A. Rigamonti, V. Tognetti, and P. Verrucchi, *ibid.* **84**, 366 (2000).

[22] Copper (deutero) formate tetrahydrate(tetradeuterate) $Cu_{1-x}Zn(Mg)_x(H(D)CO_2)H(D)_2O$, $S = 1/2$ see S.J. Clarke and A. Harrison, J. Phys. Condens. Matter, **4**, 6217 (1992); S.J. Clarke, A. Harrison, T.E. Mason, G.J. McIntyre, and D. Visser, *ibid.* **4**, L71 (1992); S.J. Clarke, A. Harrison, T.E. Mason, and D. Visser, Solid State Commun. **112**, 561 (1999).

[23] Organic-$CuCl_4$ compounds with very small exchange constants, $S = 1/2$; see P.R. Hammar, D.C. Dender, D.C. Reich, A.S. Albrecht, and C.P. Landee, J. Appl. Phys. **81**, 4615 (1997).

[24] $Mn_{1-x}Zn(Mg,Cd)_x(HCO_2)_2 2(NH_2)_2CO$, $S = 5/2$; see K. Takeda, O. Fujita, M. Hitaka, M. Mito, T. Kawae, Y. Higuchi, H.

Deguchi, Y. Muraoka, H. Kubo, M. Tokita, and K. Yamagata, J. Phys. Soc. Jpn. **69**, 3696 (2000).
[25] K. Kato, S. Todo, K. Harada, N. Kawashima, S. Miyashita, and H. Takayama, Phys. Rev. Lett. **84**, 4204 (2000).
[26] A. W. Sandvik, cond-mat/0110510 (unpublished).
[27] A.W. Sandvik, Phys. Rev. Lett. **86**, 3209 (2001); S. Todo, H. Takayama, and N. Kawashima, *ibid.* **86**, 3210 (2001).
[28] R.M. Ziff, Phys. Rev. Lett. **69**, 2670 (1992).
[29] $K_2Mn_{1-x}Mg_xF_4$, $S=5/2$; see D.J. Breed, J.W. Gilijamse, J.W.E. Sterkenburg, and A.R. Miederra, J. Appl. Phys. **41**, 1267 (1970); Physica (Amsterdam) **68**, 303 (1973); T. Idogaki and N. Uryu, J. Phys. Soc. Jpn. **45**, 1498 (1978).
[30] A.B. Harris and S. Kirkpatrick, Phys. Rev. B **16**, 542 (1977).
[31] Yu. A. Izyumov and M. V. Medvedev, *Magnetically Ordered Crystals Containing Impurities* (Consultants Bureau, New York, 1973).
[32] R.B. Stinchcombe, in *Phase Transitions and Critical Phenomena*, edited by C. Domb and J.L. Lebowitz (Academic Press, London, 1983), Vol. 7; A. Christou and R.B. Stinchcombe, J. Phys. C **19**, 5917 (1986).
[33] R. A. Tahir-Kheli, in *Phase Transitions and Critical Phenomena*, edited by C. Domb and M. S. Green (Academic Press, London, 1976), Vol. 5B, p. 259.
[34] B.I. Halperin and P.C. Hohenberg, Phys. Rev. **188**, 898 (1969).
[35] E.F. Shender, Zh. Éksp. Teor. Fiz. **75**, 352 (1978) [Sov. Phys. JETP **48**, 175 (1978)].
[36] T.A.L. Ziman, J. Phys. C **12**, 2645 (1979).
[37] C.C. Wan, A.B. Harris, and D. Kumar, Phys. Rev. B **48**, 1036 (1993).
[38] Y. Imry and S. Ma, Phys. Rev. Lett. **35**, 1399 (1975).
[39] Y.-C. Chen and A.H. Castro Neto, Phys. Rev. B **61**, R3772 (2000).
[40] E. Manousakis, Phys. Rev. B **45**, 7570 (1992).
[41] P.W. Anderson, Science **288**, 480 (2000).
[42] R.B. Laughlin and D. Pines, Proc. Natl. Acad. Sci. U.S.A. **97**, 28 (2000).
[43] A similar statement was made in Ref. 37.
[44] C. Pepin and P.A. Lee, Phys. Rev. Lett. **81**, 2779 (1998); A.A. Nersesyan, A.M. Tsvelik, and F. Wenger, *ibid.* **72**, 2628 (1994); B. Huckestein and A. Altland, cond-mat/0007413 (unpublished).
[45] L.P. Pryadko, S. Kivelson, and D.W. Hone, Phys. Rev. Lett. **80**, 5651 (1998).
[46] R.A. Cowley and W.J.L. Buyers, Rev. Mod. Phys. **44**, 406 (1972).
[47] I.Ya. Korenblit and E.F. Shender, Phys. Rev. B **48**, 9478 (1993).
[48] We use $M(x)=\Sigma_i|S_i^z|/N_m$, where N_m is the number of magnetic sites. Another physically meaningful definition counts only magnetic sites inside the infinite clusters N_m^{inf}. These definitions are connected $[M(x)=M_{inf}(x)P(x)/(1-x)]$, and at x not too close to x_p they are equivalent $[M(x)\approx M_{inf}(x)]$, since the probability of finding a magnetic site in the infinite cluster is $P(x)\simeq 1-x-\pi x^2$. Sometimes magnetization is normalized by the total number of sites N_{tot}, as in a MC study (Ref. 25). Evidently, $M_{tot}(x)=M(x)\,(1-x)$.
[49] R. A. Robinson, in *Magnetism in Heavy Fermion Systems*, edited by H. B. Radousky (World Scientific, Singapore, 2000), p. 197.
[50] M. Takahashi, Phys. Rev. Lett. **58**, 168 (1987); Phys. Rev. B **40**, 2494 (1989).
[51] A.L. Chernyshev, Y.C. Chen, and A.H. Castro Neto, Phys. Rev. Lett. **87**, 067209 (2001).
[52] D.V. Khveshchenko, A.G. Yashenkin, and I.V. Gornyi, Phys. Rev. Lett. **86**, 4668 (2001); A.G. Yashenkin, W.A. Atkinson, I.V. Gornyi, P.J. Hirschfeld, and D.V. Khveshchenko, Phys. Rev. Lett. **86**, 5982 (2001).
[53] N. Bulut, D. Hone, and D.J. Scalapino, Phys. Rev. Lett. **62**, 2192 (1989).
[54] P. Sheng, *Introduction to Wave Scattering, Localization, and Mesoscopic Phenomena* (Academic Press, San Diego, 1995).
[55] A. Junod, in *Physical Properties of High Temperature Superconductors II*, edited by D. M. Ginzberg (World Scientific, Singapore, 1990), p. 13.
[56] M. Corti, A. Rigamonti, F. Tabak, P. Carreta, F. Licci, and L. Raffo, Phys. Rev. B **52**, 4226 (1995).
[57] H.P. Van de Braak, Physica (Amsterdam) **42**, 137 (1969).
[58] M.F. Thorpe and A.R. McGurn, Phys. Rev. B **20**, 2142 (1979).
[59] A.R. McGurn, J. Phys. C **12**, 3523 (1979).
[60] V.Yu. Irkhin, A.A. Katanin, and M.I. Katsnelson, Phys. Rev. B **60**, 1082 (1999).
[61] P. Hasenfratz and F. Niedermayer, Z. Phys. B: Condens. Matter **92**, 91 (1993).
[62] A.H. Castro Neto and D. Hone, Phys. Rev. Lett. **76**, 2165 (1996).
[63] B.B. Beard, R.J. Birgeneau, M. Greven, and U.-J. Wiese, Phys. Rev. Lett. **80**, 1742 (1998); R.J. Birgeneau, M. Greven, M.A. Kastner, Y.S. Lee, B.O. Wells, Y. Endoh, K. Yamada, and G. Shirane, Phys. Rev. B **59**, 13 788 (1999).
[64] T. Nakayama, K. Yakubo, and R.L. Orbach, Rev. Mod. Phys. **66**, 381 (1994).
[65] R.A. Cowley, R.J. Birgeneau, G. Shirane, H.J. Guggenheim, and H. Ikeda, Phys. Rev. B **21**, 4038 (1980).
[66] R.J. Birgeneau, R.A. Cowley, G. Shirane, H. Yoshizawa, D.P. Belanger, A.R. King, and V. Jaccarino, Phys. Rev. B **27**, 6747 (1983).
[67] R.J. Birgeneau, R.A. Cowley, G. Shirane, J.A. Tarvin, and H.J. Guggenheim, Phys. Rev. B **21**, 317 (1980).
[68] Y.J. Uemura and R.J. Birgeneau, Phys. Rev. B **36**, 7024 (1987).
[69] G. Polatsek, O. Entin-Wohlman, and R. Orbach, Phys. Rev. B **39**, 9353 (1989).
[70] P.W. Anderson, Phys. Rev. B **109**, 1492 (1958).
[71] M.P.A. Fisher, P.B. Weichman, G. Grinstein, and D. Fisher, Phys. Rev. B **40**, 546 (1989); M.-C. Cha, M.P.A. Fisher, S.M. Girvin, M. Wallin, and A.P. Young, *ibid* **44**, 6883 (1991).
[72] P.A. Lee, Phys. Rev. Lett. **71**, 1887 (1993); C. Chamon and C. Mudry, Phys. Rev. B **63**, 100503 (2001).
[73] M. Tinkham, *Group Theory and Quantum Mechanics* (McGraw-Hill, New York, 1964).
[74] I.S. Gradshtein and I.M. Ryzhik, *Table of Integrals, Series, and Products* (Academic, New York, 1980).